琉球大学学術リポジトリ

Perfectly Matched Layers for Water Wave Absorbing Boundaries in Infinite Domain Problems

メタデータ	言語: 出版者: 琉球大学工学部 公開日: 2008-09-03 キーワード (Ja): キーワード (En): Perfectly matched layer (PML), PML equation, Complex coordinate stretching, Wave absorbing, Open boundary conditions, Infinite domain problems, Nonlinear waves, Finite element analysis 作成者: Tsutsui, Shigeaki メールアドレス: 所属:
URL	http://hdl.handle.net/20.500.12000/7127

Perfectly Matched Layers for Water Wave Absorbing Boundaries in Infinite Domain Problems

Shigeaki TSUTSUI *

Abstract

As an absorbing boundary in infinite domain problems, the perfectly matched layer (PML) is introduced to attenuate outgoing waves. The PML equation of wave propagation in a nonphysical absorbing material is derived from the governing equation with the aide of the complex coordinate stretching; both the domain of analysis and the PML are dealt with the equivalent wave equations. Because of the coordinate independence in stretching, the PML in one-dimension is essential for multidimensional problems. Through finite element computations for basic, linear and nonlinear wave propagation problems, we investigate the PML parameters to design efficient PMLs. The result shows the ability and efficiency of the PMLs for absorbing boundaries.

keywords: Perfectly matched layer (PML), PML equation, Complex coordinate stretching, Wave absorbing, Open boundary conditions, Infinite domain problems, Nonlinear waves, Finite element analysis.

1. Introduction

Problems of wave propagation and scattering in infinite domains arise from physical modeling in many fields of applications: oceanography, electromagnetics, geophysics, seismics, acoustics, and optics. For a numerical solution to a problem in an infinite domain, the computational domain must be reduced to a finite size with artificially imposed boundaries that truncate unbounded fields and must not reflect waves back. In addition, outgoing waves toward infinity are allowed as an infinite-domain solution only if they satisfy the Sommerfeld radiation condition (SRC). Taking care of this condition at infinity, therefore, the proper specification of boundary conditions along the artificial boundaries is of particular importance to simulate the wave behavior.

The interest of the present paper lies in the treatment of boundary conditions for problems of wave propagation in an unbounded coastal domain. Consider, for example, numerical experiments of water waves in an open harbor. The domain of analysis can be set up with three model boundaries: the real shoreline that consists of coastlines and the boundary lines of coastal structures, the offshore boundary in the far-field where the water depth is usually assumed to be constant, and the inshore boundary in the intermediate coastal region where the water depth varies in general; the last two are artificially imposed boundaries.

Received 20 March, 2008.

* Department of Civil Engineering and Architecture, Faculty of Eng. 1-Senbaru, Nshihara, Okinawa 903-0213 / Japan

Boundary conditions on the real shoreline are those of wave reflection and wave breaking. Along the offshore boundary in the far-field, the SRC is enforced. A typical boundary condition adopted is the transparent one that combines the numerical solution in the domain of analysis with the exterior truncated-domain solution.

One way is to discretize an exact boundary equation satisfied by outgoing waves (e.g., Yu, 1998), or to use the Dirichlet-to-Neumann (DtN) mapping that specifies the relation between the Dirichlet and the Neumann conditions along the artificial boundary (Turkel, 1998, Mesquit and Pavanello, 2005). The DtN mapping is an operator leading the exact boundary condition with desired asymptotic behavior of a solution at infinity. An alternative approach is to build an approximate boundary condition or solution based on the asymptotic behavior of outgoing waves, e.g., the series representation of the exterior solution (Chen & Mei, 1975) and the mapped infinite elements (Bettess, *et al.*, 1984; Zienkiewicz *et al.*, 1985; Chen, 1990; Park *et al.*, 1991; Chadwick *et al.*, 1999; Tsutsui, 2003). These transparent boundary conditions require usually that the artificial boundary has a particular shape, such as a circle or a circular arc, because they are designed typically for homogeneous media.

In the exterior region truncated by the inshore boundary in the intermediate coastal region, the water depth varies in general. Since neither a fundamental solution nor a series solution is known explicitly to problems with this exterior inhomogeneous region, the transparent boundary condition above cannot be formulated along the inshore boundary, and therefore only the absorbing boundary conditions are

applicable. The chief purpose of the side-conditions is to prevent the reflection of outgoing waves from the artificial boundaries. A typical approach to this is the construction of a nonphysical material with a finite thickness, placed adjacent to the model boundary; this material must attenuate perfectly outgoing waves. It is this approach that the present paper focuses on.

The sponge layer approach was introduced to absorb outgoing waves in a nonphysical material (Larsen and Dancy, 1983). Waves passing through the sponge layer are damped on the way to the artificial boundary. The sponge layer has the same roles as wave absorbers, usually laid along the sides of a two-dimensional, experimental wave-flume. Although the sponge layers have been frequently adopted in wave propagation and scattering problems, the interface between the sponge layer and the domain of analysis is not reflectionless. To be effective, therefore, the sponge layer must be designed not to reflect waves back from this interface.

To improve this unfavorable condition of sponge layers in wave absorbing problems, Bérenger (1994) invented a perfectly matched layer (PML) method for problems of electromagnetic wave propagation, governed by Maxwell's equation. The PML is a refinement of the sponge layer. Although the PML was derived for electromagnetism, the same idea works with general linear wave equations.

In the split-field PML, Bérenger's original formulation, the wave solutions are split into the sum of artificial field-components (e.g., Teixeira, *et al.* 2000; Zeng, *et al.*, 2001; Navon, *et al.*, 2004). A more common uniaxial PML expresses the PML domain as the ordinary differential equation combined with anisotropic absorbing materials (Sacks, 1995). Nowadays, both the split-field and uniaxial PML formulations are reinterpreted as a complex-valued change of coordinates, complex coordinate stretching (e.g., Chew and Weedon, 1994; Teixeira and Chew, 1997; Bindel and Govindjee, 2005). It is applicable to any linear wavelike equation (Turkel and Yefet, 1998) and only transforms the governing equation with a general way into the PML equation that governs wave propagation in a absorbing material. Thus, both the domain of analysis and the PML are dealt with the system of equivalent equations.

The PML is highly effective to absorb rapidly incident waves over a wide range of frequencies and of incident angles. Theoretically there is no spurious reflection of waves at the interface between the PML and the domain of analysis; that is, the PML perfectly matches the rest of the domain. This zero-reflection allows a more effective absorbing boundary than the classical sponge layer. From the numerical examinations of wave absorption in various fields, the PML approaches have been shown to provide significantly better accuracy than the other artificial boundary conditions.

With respect to absorbing boundary conditions in the field of coastal engineering, since the proposal of sponge layers, the sponge layer and its variants combined with the SRC have been adopted widely and successfully in wave propagation and scattering problems (e.g., Yamashita *et al.*, 1990; Ohyama and Nadaoka, 1990; Wei and Kirby, 1995; Gobbi and Kirby, 1999; Abohadima *et al.*, 1999; Akikawa and Isobe, 1999; Lee and Yoon, 2004). Another approaches are the construction of absorbing material that work with the linear term in the governing equation, the same as the energy dissipation term due to wave breaking and bottom friction (e.g., Sato *et al.*, 1988; Kubo *et al.*, 1992; Ishii *et al.*, 1994; Cruz *et al.*,1993, 1997). To date, however, there has been relatively little analysis of the PML equation. Under the circumstances, a treatment of the open boundary condition in the finite difference scheme (Kiyokawa *et al.*, 1996) is similar to the concept in the PML methodology; this boundary condition has to be dealt with the equation equivalent to the governing equation.

The present paper introduces typical PMLs available to problems of wave-deformation in infinite domains. The PML method is applicable to the nonlinear wave equation implemented, coastal wave-deformation model (Tsutsui *et al.*, 1996, 1998; Tsutsui and Ohki, 1998; Tsutsui, 2003), because its linear terms are the mild-slope equation. The complex coordinate stretching, applicable to the linear wave system, results in the PML equation.

Although the main interest of numerical simulations lies in multidimensional problems, in deriving a PML equation for an absorbing material in two-dimension, we can use the PML methodology in one-dimension. When the problem is posed in the Cartesian coordinates, we can stretch each Cartesian component independently based on the complex coordinate stretching. Consequently, the clarification of the PML characteristics in one-dimension is of particular significance in design of multidimensional PMLs.

Based on the finite element method (FEM), the one-dimensional numerical experiments of the coastal wave-deformation model combined with the PMLs is presented for some basic problems of linear and nonlinear wave propagation. Through these experiments, we make clear the effects of domain discretization and PML parameters on the wave absorbing characteristics, and then give guidelines to design the PMLs. The result shows ability and efficiency of the present technique with the PMLs for nonlinear wave simulation in unbounded coastal domains.

2. Complex Coordinate Stretching and PML Equation

When specifying appropriate boundary conditions along the boundaries imposed artificially to reduce the size of the computational domain, we make simplifications to the space far from the domain of analysis:

- Bathymetric homogeneity; a constant water depth.
- Linearity and time-invariance; linear and steady state conditions for a wave field.

Under these assumptions, the governing equation for linear water waves in a domain of constant water depth is the Helmholtz equation:

$$\left(\frac{\partial^2}{\partial x^2}+\frac{\partial^2}{\partial y^2}\right)\zeta + k^2\zeta = 0, \tag{2.1}$$

where (x,y) are the horizontal space variables, the coordinate origin being on the still water level, ζ is the free surface displacement, and k is the wave number. For a solution to infinite domain problems, the SRC in the far-field must be enforced to make the Helmholtz problem well-posed, i.e.,

$$\lim_{r\to\infty} r^{\frac{d-1}{2}}\left(\frac{\partial\zeta}{\partial r}+ik\zeta\right)=0, \tag{2.2}$$

where r is the distance from the origin of disturbances, d is the dimension of the wave field, and $i=(-1)^{1/2}$ is the imaginary unit.

The Helmholtz equation in one-dimension is

$$\frac{d^2\zeta}{dx^2}+k^2\zeta=0, \tag{2.3}$$

where the wave properties are independent of y. If the time dependence is assumed to be $\exp(i\omega t)$, where t is the time and ω is the frequency, a particular solution to Eq. (2.3) with the SRC is given by

$$\zeta = a\exp(-ikx), \tag{2.4}$$

where a is an amplitude. Note that this wave propagates toward $x\sim+\infty$ in the time dependence here.

Consider the change of coordinates in Eqs. (2.3) and (2.4). The key concept is that since the solution (2.4) is an analytical function of the real x, it is continued analytically to the complex value; similarly, Eq. (2.3) is also continued analytically. By the analytical continuation, therefore, it holds that

$$\frac{d^2\zeta}{dz^2}+k^2\zeta=0, \tag{2.5}$$

$$\zeta = a\exp(-ikz), \tag{2.6}$$

in the complex variable $z=x-iy$ †.

The original problem corresponds to the real axis of z, and then in this case Eq. (2.6) gives an oscillating solution $\exp(-ikx)$. Along the contour in the complex z-plane where the imaginary part y takes nonzero values, the solution becomes $\exp(-ikx-ky)$, showing exponential decay with respect to the increase in y; i.e., the solution in the region for $y>0$ acts like the solution in an absorbing material.

Figure 2.1 shows an example of the result of complex coordinate stretching described above:

(1) The linearly deformed contour:
$y=0$ for $x\le 5$; $y>0$ for $x>5$.

(2) The solution doesn't change in the region for $x\le 5$ with no-deformation but, because of the stretching of the contour, it decays exponentially in the region for $x>5$ that corresponds to an absorbing region. This is the solution we are interested in.

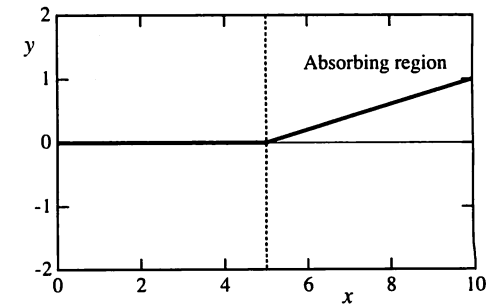

(1) Deformed contour; linearly increasing y.

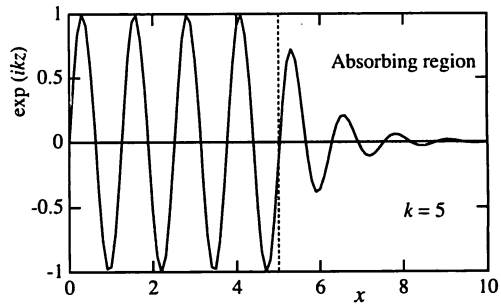

(2) Solution (k = 5).

Figure 2.1. Deformed contour in the complex z-plane and the decay of an oscillating solution.

Note that the analytically continued solution (2.6) satisfies the differential equation (2.5) with the same form as the original equation (2.3). A crucial difference from usual absorbing materials, such as sponge layers, is that the deformed contour in the z-plane acts like an absorbing and reflectionless material; this is a PML.

The only problem, however, is that solving differential equations along contours in the complex z-plane is rather inconvenient than that in the real x. To fix this difficulty, we have to use the variable x in place of z. In doing so, it is convenient that the imaginary part of z is a function of x:

$$z = x - if(x), \tag{2.7}$$

where $f(x)$ is a function that indicates how the contour is deformed with the real x-axis. The analytically continued equation has a differential and then $dz=(1-idf/dx)\,dx$. The relation $df/dx=\varphi(x)/k$ is preferable for water wave problems because of the form of solution (2.6). Now, define the continuous, complex-valued function so that

$$\lambda(x)=1-i\frac{df(x)}{dx}=1-\frac{i}{k}\varphi(x), \tag{2.8}$$

and thus the following relations hold:

$$\left.\begin{aligned} z&=\int_0^x\lambda(s)ds=x-\frac{i}{k}\rho(x)\\ \rho(x)&=\int_0^x\varphi(s)ds\end{aligned}\right\}, \tag{2.9}$$

$$\zeta = a\exp(-ikz)=a\exp\{-ikx-\rho(x)\}, \tag{2.10}$$

where $\rho(x)$ is the attenuation rate.

† The sign of the imaginary part y depends on the sign of the time factor.

In the example demonstrated in Fig. 2.1 (1), $\varphi(x)$ is a step function; i.e., zero for $x \leq 5$ because of $f(x) = 0$ and a positive constant for $x > 5$ because $f(x)$ is a linearly increasing function. In Fig. 2.1 (2), analytically, there is no reflection at the interface $x = 5$ between these two regions because the solution is only an analytical continuation of the original solution from x to z.

In the analytical region of interest where $\varphi = 0$, the wave equation and thus the oscillating solution are unchanged; in the absorbing region where $\varphi > 0$, the solution turns into exponentially decaying one. Therefore, φ is termed an attenuation function, and the region for $\varphi > 0$ a perfectly matched medium (PMM), where the outgoing wave decays exponentially. Therefore, the design of the attenuation function φ is of importance for the PML.

The differential relation between z and x is

$$\frac{d}{dz} = \frac{1}{\lambda(x)} \frac{d}{dx}, \tag{2.11}$$

and therefore the equation (2.5) becomes

$$\frac{1}{\lambda} \frac{d}{dx}\left(\frac{1}{\lambda} \frac{d\zeta}{dx}\right) + k^2 \zeta = 0. \tag{2.12}$$

The transformed equation (2.12) is the PML equation that governs wave propagation in a PMM. The general solution to this equation is given as

$$\begin{aligned} \zeta &= a_{\text{in}} \exp(ikz) + a_{\text{out}} \exp(-ikz) \\ &= a_{\text{in}} \exp\{\rho(x)\} \exp(ikx) \\ &\quad + a_{\text{out}} \exp\{-\rho(x)\} \exp(-ikx), \end{aligned} \tag{2.13}$$

where a_{in} and a_{out} are the amplitudes of incoming and outgoing waves. So long as $\varphi(s) = 0$ and thus $\rho(x) = 0$, the solution (2.13) agrees with the solution to the original Helmholtz equation (2.3). When $\varphi(s) > 0$, the outgoing wave decays with $\exp\{-\rho(x)\}$, and the incoming wave grows with $\exp\{\rho(x)\}$. Conceptually, the process above based on the analytical continuation indicates a simple transformation of the original differential equation through the correspondence:

$$\frac{\partial}{\partial x} \longleftrightarrow \frac{1}{\lambda(x)} \frac{\partial}{\partial x}. \tag{2.14}$$

For the two-dimensional Helmholtz equation (2.1), the PML equation is obtained in the same way as in the one-dimensional problem. For convenience in handling the system, we can assume that the complex-valued function λ_1 depends only on x and λ_2 only on y. We can therefore stretch each Cartesian component independently, and the two-dimensional analogue to Eq. (2.14) is given by

$$\frac{\partial}{\partial x} \longleftrightarrow \frac{1}{\lambda_1(x)} \frac{\partial}{\partial x}, \quad \frac{\partial}{\partial y} \longleftrightarrow \frac{1}{\lambda_2(y)} \frac{\partial}{\partial y}. \tag{2.15}$$

Thus, Eq. (2.1) is transformed into

$$\frac{1}{\lambda_1} \frac{\partial}{\partial x}\left(\frac{1}{\lambda_1} \frac{\partial \zeta}{\partial x}\right) + \frac{1}{\lambda_2} \frac{\partial}{\partial y}\left(\frac{1}{\lambda_2} \frac{\partial \zeta}{\partial y}\right) + k^2 \zeta = 0, \tag{2.16}$$

Multiplying Eq. (2.16) by $\lambda_1(x)\lambda_2(y)$ results in

$$\frac{\partial}{\partial x}\left(\frac{\lambda_2}{\lambda_1} \frac{\partial \zeta}{\partial x}\right) + \frac{\partial}{\partial y}\left(\frac{\lambda_1}{\lambda_2} \frac{\partial \zeta}{\partial y}\right) + \lambda_1 \lambda_2 k^2 \zeta = 0. \tag{2.17}$$

The equations (2.12) and (2.17) are interpreted as the equations for waves in an inhomogeneous and anisotropic material; the PMLs used in computational wave dynamics can similarly be interpreted as layers with specially-tuned values for the constitutive parameters. Furthermore, due to the coordinate independence in the complex coordinate stretching, the clarification of the PML characteristics in one-dimension is of especial significance in design of multidimensional PMLs.

3. One-Dimensional PML

3.1 *Right-PML*

Consider plane-wave propagation in an unbounded domain extend to $x = \pm\infty$. Incident waves arriving from $x \sim +\infty$ are scattered by obstacles in the domain of analysis; some of the scattered waves are reflected back to $x \sim +\infty$, and the rest are transmitted toward $x \sim -\infty$. For the solution to this problem, we must truncate both sides of the domain of analysis by the PMLs on the x-axis. The first truncation model is setting up of the right-PML to absorb outgoing waves toward $x \sim +\infty$. The term "right" means that the PML is set up on the right-hand side of the domain of analysis, as shown in Figs. 3.1 and 3.2.

A. Power PML

Suppose that the attenuation function $\varphi(s)$ is defined by a power function:

$$\varphi(s) = \begin{cases} 0 & [0, R] \\ \beta(m+1)\left(\dfrac{s-R}{D}\right)^m & [R, R_p] \end{cases}, \tag{3.1}$$

with $D \equiv R_p - R$, where the bounded domain of analysis is $[0, R]$, next to this domain the right-PML is set up in the interval $[R, R_p]$, as in Fig. 3.1, D is a PML thickness, m is an index of powers, and β is a scaling parameter. In this PML, the profiles for $m = 1$ and 2 are usually used in various fields, such as electromagnetics and acoustics.

The deformed contour is

$$z = x - \frac{i}{k} \rho(x), \tag{3.2}$$

with the attenuation rate:

$$\rho(x) = \int_0^x \varphi(s)\, ds = \beta D^{-m} (x - R)^{m+1}. \tag{3.3}$$

Note that this contour is continuous and its imaginary part takes the value zero at the interface $x = R$ between the PML and the domain of analysis because of $\rho(R) = 0$.

The waves are given, from Eq. (2.13), as

$$\zeta = \begin{cases} a_{\text{in}} \exp(ikx) + a_{\text{out}} \exp(-ikx), & 0 \leq x \leq R \\ a_{\text{in}} \exp\{\rho(x)\} \exp(ikx) & \\ \quad + a_{\text{out}} \exp\{-\rho(x)\} \exp(-ikx), & R \leq x \leq R_p \end{cases} \tag{3.4}$$

and are continuous at the interface $x = R$ because of

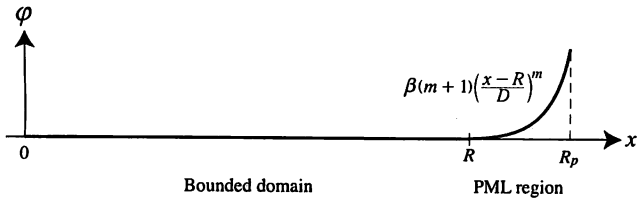

Figure 3.1. Piece-wise power attenuation function, set up in the interval $[R, R_p]$.

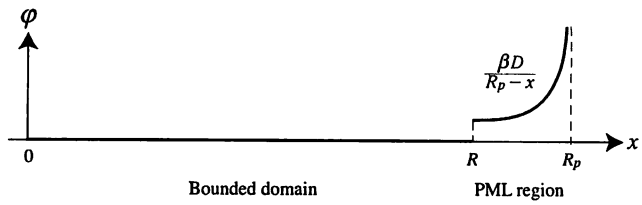

Figure 3.2. Piece-wise singular attenuation function, set up in the interval $[R, R_p]$.

$\rho(R) = 0$. In the PML, $x > R$, the outgoing wave from the origin toward $x \sim +\infty$ decays like $\exp\{-\rho(x)\}$. This decaying property in the PML is written as

$$\Phi = \exp\left\{-\gamma\left(\frac{\xi}{D}\right)^{m+1}\right\}, \tag{3.5}$$

with $\xi = x - R$ and $\gamma = \beta D$.

To specify the reflection and transmission coefficients at the end-side of the PML, $x = R_p$, if we prescribe $\zeta(0) = 1$ for input and $\zeta(R_p) = 0$ for output, the boundary conditions become

$$\left.\begin{aligned} &a_{\text{in}} + a_{\text{out}} = 1 \\ &a_{\text{in}} \exp(\gamma)\exp(ikR_p) + a_{\text{out}} \exp(-\gamma)\exp(-ikR_p) = 0 \end{aligned}\right\}, \tag{3.6}$$

and the coefficients a_{in} and a_{out} are thus evaluated by

$$\begin{aligned} a_{\text{in}} &= -\frac{\exp(-2\gamma)\exp(-2ikR_p)}{1 - \exp(-2\gamma)\exp(-2ikR_p)} \\ &\fallingdotseq -\exp(-2\gamma)\exp(-2ikR_p), \end{aligned} \tag{3.7.1}$$

$$\begin{aligned} a_{\text{out}} &= \frac{1}{1 - \exp(-2\gamma)\exp(-2ikR_p)} \\ &\fallingdotseq 1 + \exp(-2\gamma)\exp(-2ikR_p). \end{aligned} \tag{3.7.2}$$

The wave in the PML is approximated by

$$\begin{aligned} \zeta \fallingdotseq &-\exp\{-2\gamma + \rho(x)\}\exp(ikx - 2ikR_p) \\ &+\exp\{-\rho(x)\}\exp(-ikx), \end{aligned} \tag{3.8}$$

and $\rho(x) = \gamma$ as $x \to R_p$. Therefore, both the reflection and transmission coefficients are given by

$$|R| = \exp(-\gamma) \quad \text{with } \gamma = \beta D. \tag{3.9}$$

B. Singular PML

If a singular attenuation function (Bermúdez *et al.*, 2004):

$$\varphi(s) = \begin{cases} 0 & [0, R] \\ \dfrac{\beta D}{R_p - s} & [R, R_p] \end{cases} \tag{3.10}$$

is used as the right-PML, as shown in Fig. 3.2, the attenuation rate is

$$\rho(x) = \int_0^x \varphi(s)\, ds = \beta D \log\frac{D}{R_p - x}. \tag{3.11}$$

As is in the power PML, this contour is continuous, and its imaginary part takes the value zero at the interface $x = R$ between the PML and the domain of analysis. Therefore, the following relations hold.

- Waves:

$$\zeta = \begin{cases} a_{\text{in}} \exp(ikx) + a_{\text{out}} \exp(-ikx), & 0 \le x \le R \\ a_{\text{in}} \exp\{\rho(x)\}\exp(ikx) & \\ \quad + a_{\text{out}} \exp\{-\rho(x)\}\exp(-ikx), & R \le x \le R_p \end{cases} \tag{3.12}$$

- Decaying property:

$$\Phi = \exp\left(-\gamma \log\frac{1}{1 - \xi/D}\right), \tag{3.13}$$

with $\xi = x - R$ and $\gamma = \beta D$.

- Coefficients a_{in} and a_{out}:

The prescriptions $\zeta(0) = 1$, $\zeta(x_0) = 0$, and $\rho(x_0) \to -\infty$ as $\Delta x \to 0$ $(x_0 = R_p - \Delta x)$ give

$$a_{\text{in}} = -\frac{\exp\{-2\rho(x_0)\}\exp(-2ikx_0)}{1 - \exp\{-2\rho(x_0)\}\exp(-2ikx_0)} = 0, \tag{3.14.1}$$

$$a_{\text{out}} = \frac{1}{1 - \exp\{-2\rho(x_0)\}\exp(-2ikx_0)} = 1. \tag{3.14.2}$$

- Wave in the PML:

$$\zeta = \exp\{-\rho(x)\}\exp(-ikx). \tag{3.15}$$

- Reflection and transmission coefficients:

$$|R| = \lim_{x \to R_p} \exp\left(-\gamma \log\frac{D}{R_p - x}\right) = 0. \tag{3.16}$$

3.2 *Left-PML*

The second truncation model on the x-axis is setting up of the left-PML to absorb transmitted waves propagating toward $x \sim -\infty$. The term "left" means that the PML is set up on the left-hand side of the domain of analysis.

A. Power PML

As shown in Fig. 3.3, the left-PML is set up in the interval $[R_p, R]$, next to the domain of analysis $[R, R_\infty]$. The attenuation function $\varphi(s)$ is defined by a power function:

$$\varphi(s) = \begin{cases} 0 & [R, R_\infty] \\ \beta(m+1)\left(\dfrac{R - s}{D}\right)^m & [R_p, R] \end{cases}, \tag{3.17}$$

with $D \equiv R - R_p$. The attenuation rate is

$$\rho(x) = \int_{R_\infty}^x \varphi(s)\, ds = -\beta D^{-m}(R - x)^{m+1}. \tag{3.18}$$

The waves are given, from Eq. (2.13), as

$$\zeta = \begin{cases} a_{\text{in}} \exp(ikx) + a_{\text{out}} \exp(-ikx), & R \le x \le R_\infty \\ a_{\text{in}} \exp\{\rho(x)\}\exp(ikx) & \\ \quad + a_{\text{out}} \exp\{-\rho(x)\}\exp(-ikx), & R_p \le x \le R \end{cases} \tag{3.19}$$

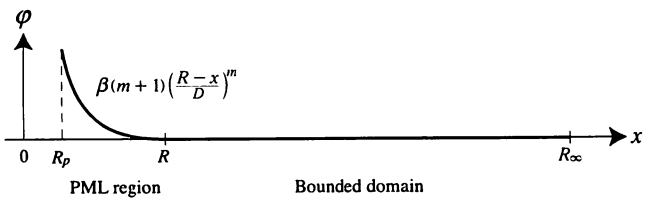

Figure 3.3. Piece-wise power attenuation functions, set up in the interval $[R_p, R]$.

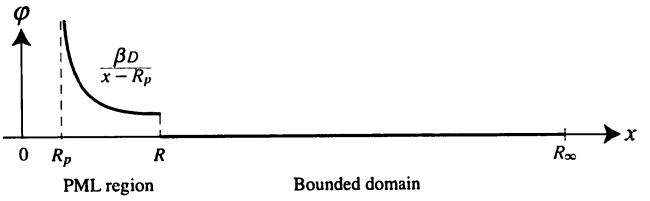

Figure 3.4. Piece-wise singular attenuation function, set up in the interval $[R_p, R]$.

and are continuous at the interface $x = R$ because of $\rho(R) = 0$. In the PML, $x < R$, the outgoing wave from $x = R_\infty$ toward $x \sim -\infty$ decays like $\exp\{\rho(x)\}$. This decaying property in the PML is written as

$$\Phi = \exp\left\{-\gamma\left(\frac{\xi}{D}\right)^{m+1}\right\}, \tag{3.20}$$

with $\xi = R - x$ and $\gamma = \beta D$.

To specify the reflection and transmission coefficients at the end-side of the PML, $x = R_p$, we prescribe $\zeta(R) = 1$ for input and $\zeta(R_p) = 0$ for output. The boundary conditions become

$$\left.\begin{aligned} &a_{\text{in}} \exp(ikR) + a_{\text{out}} \exp(-ikR) = 1 \\ &a_{\text{in}} \exp(-\gamma) \exp(ikR_p) + a_{\text{out}} \exp(\gamma) \exp(-ikR_p) = 0 \end{aligned}\right\}, \tag{3.21}$$

and the coefficients a_{in} and a_{out} are thus evaluated by

$$\begin{aligned} a_{\text{in}} &= \frac{\exp(-ikR)}{1 - \exp(-2\gamma)\exp(2ikR_p)\exp(-2ikR)} \\ &\fallingdotseq \exp(-ikR) + \exp(-2\gamma)\exp(2ikR_p)\exp(-3ikR), \end{aligned} \tag{3.22.1}$$

$$\begin{aligned} a_{\text{out}} &= -\frac{\exp(-2\gamma)\exp(2ikR_p)\exp(-ikR)}{1 - \exp(-2\gamma)\exp(2ikR_p)\exp(-2ikR)} \\ &\fallingdotseq -\exp(-2\gamma)\exp(2ikR_p)\exp(-ikR). \end{aligned} \tag{3.22.2}$$

Because of the first boundary condition in Eq. (3.21), the phase-shift arises in Eq. (3.22). The wave in the PML is approximated by

$$\begin{aligned} \zeta \fallingdotseq\ &\exp\{\rho(x)\}\exp(ikx - ikR) \\ &-\exp\{-2\gamma - \rho(x)\}\exp(-ikx - ikR)\exp(2ikR_p), \end{aligned} \tag{3.23}$$

and $\rho(R_p) = -\gamma$ as $x \to R_p$. Therefore, the reflection and transmission coefficients are given by

$$|R| = \exp(-\gamma) \quad \text{with } \gamma = \beta D. \tag{3.24}$$

B. Singular PML

Similar to the power PML, the singular PML is set up in the interval $[R_p, R]$, the left-hand side of the domain of analysis $[R, R_\infty]$, as shown in Fig. 3.4. If the singular attenuation function with the PML thickness D

$$\varphi(s) = \begin{cases} 0 & [R, R_\infty] \\ \dfrac{\beta D}{s - R_p} & [R_p, R] \end{cases} \tag{3.25}$$

is used, the attenuation rate is

$$\rho(x) = \int_{R_\infty}^{x} \varphi(s)\, ds = \beta D \log\frac{x - R_p}{D}. \tag{3.26}$$

Therefore, the following relations hold.

- Waves:

$$\zeta = \begin{cases} a_{\text{in}} \exp(ikx) + a_{\text{out}} \exp(-ikx), & R \le x \le R_\infty \\ a_{\text{in}} \exp\{\rho(x)\} \exp(ikx) \\ \quad + a_{\text{out}} \exp\{-\rho(x)\} \exp(-ikx), & R_p \le x \le R \end{cases} \tag{3.27}$$

- Decaying property:

$$\Phi = \exp\left\{-\gamma \log\frac{1}{1 - \xi/D}\right\}, \tag{3.28}$$

with $\xi = R - x$ and $\gamma = \beta D$.

- Coefficients a_{in} and a_{out}:

The prescriptions $\zeta(R) = 1$, $\zeta(x_0) = 0$, and $\rho(x_0) \to -\infty$ as $\Delta x \to 0$ $(x_0 = R_p + \Delta x)$ give

$$\begin{aligned} a_{\text{in}} &= \frac{\exp(-ikR)}{1 - \exp\{2\rho(x_0)\}\exp(2ikx_0)\exp(-2ikR)} \\ &= \exp(-ikR), \end{aligned} \tag{3.29.1}$$

$$a_{\text{out}} = -\frac{\exp\{2\rho(x_0)\}\exp(2ikx_0)\exp(-ikR)}{1 - \exp\{2\rho(x_0)\}\exp(2ikx_0)\exp(-2ikR)} = 0. \tag{3.29.2}$$

- Wave in the PML:

$$\zeta = \exp\{\rho(x)\}\exp(ikx - ikR). \tag{3.30}$$

- Reflection and transmission coefficients:

$$|R| = \lim_{|x| \to R_p} \exp\left\{-\gamma \log\frac{1}{1 - \xi/D}\right\} = 0. \tag{3.31}$$

3.3 *Wave reflection and the scaling parameter*

The incident wave to the PML with the thickness D will give rise to two reflected waves from the boundaries of the PML, as shown in Fig. 3.5:

- Discretization-waves or numerical-waves reflected at the interface, $\xi = 0$.
- PML-waves reflected at the end-side, $\xi = D$.

Theoretically, the PML is reflectionless if we are solving the exact wave equation. As soon as discretized, however, we are solving an approximate wave equation, and thus the interface between the PML and the domain of analysis is no longer reflectionless. As a result, the reflection of discretization-waves occurs, but may be small because the discretization is presumably a good approximation to the exact wave equation. Thus, with the aid of the appropriate

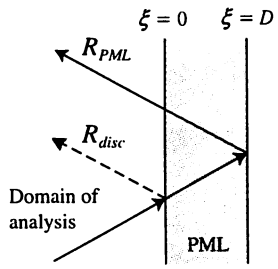

Figure 3.5. Reflection of waves at the boundaries of the PML.

discretization, it becomes small.

For the PML-waves, the reflection coefficient in the power PML is generally given by

$$|R| = \exp(-\gamma), \tag{3.32}$$

where $\gamma = \beta D$. In implementation of the power PML in finite element computations, the PML thickness D has to be designed when discretizing the domain of analysis, together with the reflection coefficient $|R|$, and therefore the scaling parameter is specified by $\beta = \gamma/D$. If γ is too large, however, the wave decays so quickly on the way to the end-side of the PML that many nodal points in the PML are required to achieve an accurate discretization for this quick decay.

For the singular PML, on the contrary, there is no relation between PML parameters because the reflection of PML-waves is always zero, i.e., $|R| = 0$. Further, the optimal parameter β depends on the finite element mesh size and the properties of the problem (Bermúdez *et al.*, 2004).

3.4 *Comparison of PMLs*

First, we discuss the basic characteristics of power PMLs with the parameters $m = 0$ (constant), 1 (linear), and 2 (quadratic). Figure 3.6 (1) shows the decaying properties (3.5) in the right-PMLs for various values of $\gamma = \beta D$.

Since, in order for a PML to be an absorbing material, the outgoing wave height must decrease to zero when approaching the end-side of the PML, the PML for large values of γ has a possibility to be a wave absorber. For large values of γ, the constant PML linearly absorbs waves near the interface at $\xi = 0$ between the PML and the domain of analysis. Linear and quadratic PMLs show gradual decaying properties near the interface. For higher powers, this property becomes remarkable. After that, the PMLs sharply attenuate outgoing waves on the way to the end-side $\xi = D$ of the PML.

If the reflection coefficient in the power PMLs is negligibly small, i.e., $\exp(-\gamma) \ll 1$, the outgoing waves in the domain of analysis and the PML can be written, from Eqs. (3.4) and (3.7), as

$$\zeta \fallingdotseq \begin{cases} \exp(-ikx), & 0 \le x \le R \\ \exp\{-\rho(x)\}\exp(-ikx), & R \le x \le R_p \end{cases}, \tag{3.33}$$

where the attenuation rate $\rho(x)$ is given by Eq. (3.3). Figure 3.6 (2) shows examples of decaying wave profiles (3.33), in which the right-PMLs are set up in the interval $[R, R_p] = [5, 10]$ and $\gamma = 5$ decided from Fig. 3.6 (1) so as to satisfy the condition $\exp(-\gamma) \ll 1$. Difference in wave decaying properties due to PMLs appears clearly.

Compared with the sudden absorption of waves in the constant PML, which occurs near the interface $x = R = 5$ $(\xi = 0)$ between the PML and the domain of analysis, the gradual absorption of waves in linear and quadratic PMLs is favorable to prevent the reflection of discretization-waves at $\xi = 0$. The reason alluded briefly to this point is as follows: This reflection can be made small as long as the medium in the PML (the deformed contour) is slowly varying because of an adiabatic theorem (Johnson *et al.*, 2002). To prevent the reflection of discretization-waves, therefore, the PML must be an anisotropic absorber turned on gradually and smoothly enough.

For appropriate values of γ, the bounded solution, such as Eq. (3.4), can be an approximation to the solution in the infinite domain. Since the reflection coefficient for PML-waves at the end-side of the power PML is given by Eq. (3.32), $\exp(-4.6) \fallingdotseq 0.01$, and $\exp(-6.9) \fallingdotseq 0.001$, these two values of γ are standard values to make the reflection of PML-waves less than 1%. In practice, especially for nonlinear wave propagation, it has to be specified through the numerical experiments because wave decaying properties depend on the finite element mesh.

A replacement of the far-field condition analogous to the SRC in one-dimension, i.e., $d = 1$ in Eq. (2.2), is that a solution must decay to zero as $x \to \infty$; a corresponding approximation is obtained if we enforce $\zeta(R_p) = 0$ at the end-side of the PML. This condition is also useful to suppress the reflection of PML-waves at the end-side of the PML.

Similarly, Fig. 3.7 shows the decaying properties in the singular right-PML, given by Eq. (3.13), and an example of wave profiles decaying in the PML, approximated by Eqs. (3.11) and (3.33), where $\gamma = 5$. The singular PML is a special absorbing material because it always achieves $\Phi \to 0$, i.e., $|R| \to 0$ at the end-side of the PML, $\xi = D$. For small values of γ, outgoing waves are absorbed gradually near $\xi = 0$ and quickly in the region very close to $\xi = D$. For large values of γ, the singular PML linearly absorbs waves near the interface at $\xi = 0$, as was in the constant PML.

To implement the singular PML, however, element integrals with the discontinuous function are required, though the integrals are bounded. In addition, as described before, the optimal parameter β depends on the finite element mesh and the properties of the problem. These are disadvantages for the use of the singular PML. Therefore, in the following discussions, we adopt the power PMLs as absorbing materials.

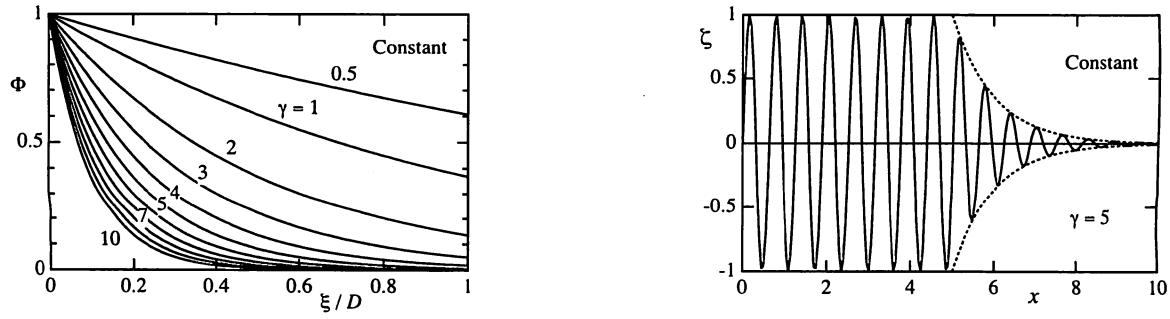

(a) PML with a constant attenuation function.

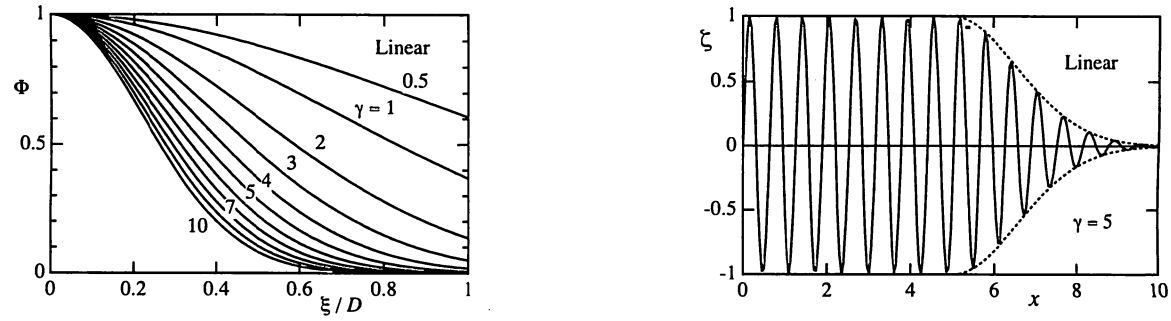

(b) PML with a linear attenuation function.

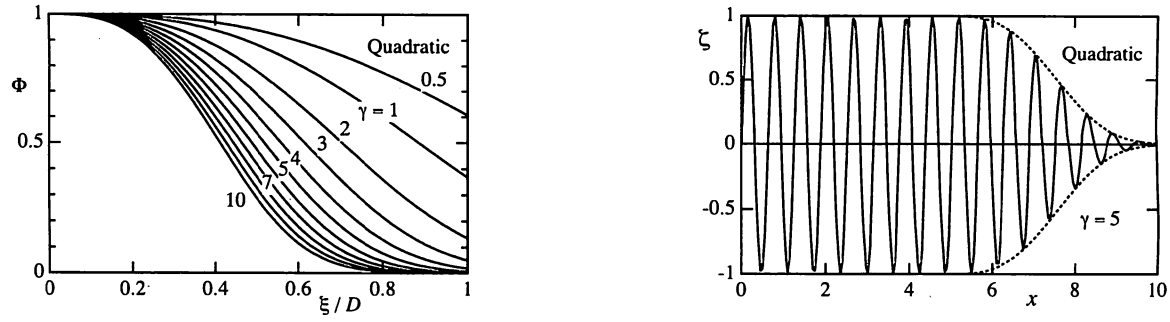

(c) PML with a quadratic attenuation function.

(1) Decaying property. (2) Waves in the PML.

Figure 3.6. Wave decaying property and wave profiles in the power PMLs.

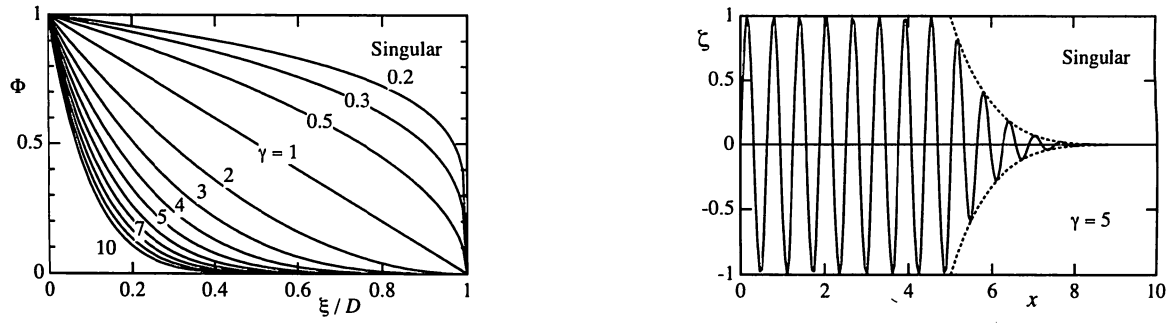

(1) Decaying property. (2) Waves in the PML.

Figure 3.7. Wave decaying property and wave profiles in the singular PML.

4. Weak Form for FEM

4.1 *Two-dimensional problems*

For a numerical solution to a problem of wave propagation and scattering in an infinite domain, the computational domain must be reduced to a finite size with artificially

imposed boundaries that truncate the unbounded far-field. The domain of wave analysis is therefore subdivided into two domains, Ω and Ω_∞, by the boundary Γ, as shown in Fig. 4.1, where the region of nonlinear wave analysis, Ω_n, is included in Ω. The infinite domain Ω_∞ surrounds the domain Ω and expands to infinity.

In the wave-deformation modeling, the water depth in Ω_∞ is usually assumed to be constant to easily handle the far-field boundary condition, but this restriction is released here to deal with the actual bathymetric condition, i.e., the water depth in Ω_∞ may vary. For example, in the harbor model in Fig. 4.1 (b), the water depth in front of the coast line varies. In doing so, the domain Ω_∞ is further truncated by using the PML with a finite width denoted by the boundaries Γ to Γ_∞; the PML is used as an absorbing material for outgoing waves that enter into the PML and are attenuated on the way toward the end-side of the PML, denoted by the broken line Γ_∞.

Waves in Ω are governed by the model equation for wave-deformation, Eq. (A.3), resulting from application of the Fourier spectral method to the equation of continuity and the momentum equations of motion. Waves in the PML, a part of Ω_∞, are governed by the PML equation, Eq. (A.7.2). Consider the case that, in the domain Ω, there may be the boundary Γ_B, such as coast lines and artificial structures, and the lines of water depth discontinuity Γ_D, such as boundaries of dredged regions and reef coasts.

The governing equations and the boundary conditions are given in **Appendix**; they are written as follows:

$$\nabla\cdot(cc_g\nabla\zeta)+(m\omega)^2\left(\frac{c_g}{c}-\frac{i}{m\omega}f_d\right)\zeta=Q \quad \text{in } \Omega, \tag{4.1}$$

$$\nabla_1\left(\frac{\lambda_2}{\lambda_1}cc_g\nabla_1\zeta^\infty\right)+\nabla_2\left(\frac{\lambda_1}{\lambda_2}cc_g\nabla_2\zeta^\infty\right)$$
$$+(m\omega)^2\left(\frac{c_g}{c}-\frac{i}{m\omega}f_d\right)\lambda_1\lambda_2\zeta^\infty=0 \quad \text{in } \Omega_\infty, \tag{4.2}$$

$$\zeta=\zeta^\infty, \quad \boldsymbol{n}\cdot\nabla\zeta+\boldsymbol{n}_\infty\cdot\nabla\zeta^\infty=0 \quad \text{on } \Gamma, \tag{4.3}$$

$$\boldsymbol{n}_B\cdot\nabla\zeta=B\zeta \quad \text{on } \Gamma_B, \tag{4.4}$$

$$\left[cc_g\boldsymbol{n}_D\cdot\nabla\zeta\right]_{\xi_0^-}^{\xi_0^+}=D\zeta \quad \text{on } \Gamma_D, \tag{4.5}$$

Sommerfeld's radiation condition at infinity. (4.6)

Equation (4.2) is the PML equation for the mild-slope equation in Ω_∞, where $(\nabla_1,\nabla_2)=(\partial/\partial x,\partial/\partial y)$. At the interface Γ between the domain of analysis and the PML, both λ_1 and λ_2 take the value unity, and thus in this case Eq. (4.2) is identical to the mild-slope equation.

The significance in the model above with the use of PMLs is that the whole domain $\Omega+\Omega_\infty$ of finite element discretization is governed by the system of equivalent equations because the PML equation applied to wave absorbing materials in Ω_∞ is the linearized version of the governing equation to the domain of analysis Ω.

The weak form for FEM is described for the system of governing equations and boundary conditions, Eqs. (4.1)-(4.5); Eq. (4.6) is satisfied in implementing the PML in the domain Ω_∞. The domain integrals for the product of a

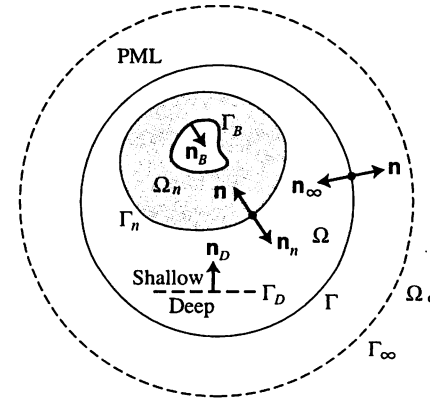

(a) Islands model

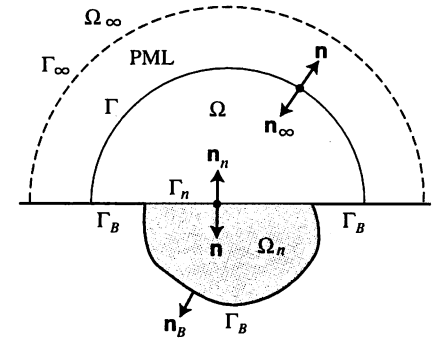

(b) Harbor model.

Fig. 4.1. Model definition with the absorbing boundaries by the PML.

shape function and the governing equations, Eqs. (4.1) and (4.2), are transformed, with the aid of Green's formula, into the weak forms. Furthermore, satisfying the boundary conditions in the curvilinear integrals obtained from Eqs. (4.3)-(4.5), we can eliminate the derivatives of free surface displacement, $\nabla\zeta$ and $\nabla_j\zeta^\infty$. As a result (**Appendix**), the weak form becomes

$$\iint_\Omega\left\{cc_g\nabla v_1\cdot\nabla\zeta-v_1(m\omega)^2\left(\frac{c_g}{c}-\frac{i}{m\omega}f_d\right)\zeta+v_1Q\right\}d\Omega$$
$$+\iint_{\Omega_\infty}\begin{bmatrix}\frac{\lambda_2}{\lambda_1}cc_g\nabla_1v_1\,\nabla_1\zeta^\infty+\frac{\lambda_1}{\lambda_2}cc_g\nabla_2v_1\,\nabla_2\zeta^\infty\\-v_1(m\omega)^2\left(\frac{c_g}{c}-\frac{i}{m\omega}f_d\right)\lambda_1\lambda_2\zeta^\infty\end{bmatrix}d\Omega_\infty$$
$$-\int_{\Gamma_B}v_1cc_gB\zeta ds-\int_{\Gamma_D}v_1D\zeta ds=0, \tag{4.7}$$

where v_1 is the shape function.

This is the equation for an equilibrium state of wave field. Since there is no source function that generates an incident wave to the domain of analysis, it must be added in the right-hand side of Eq. (4.7) as an external force. If the water depth varies in Ω_∞, as in a general bathymetric condition, waves being incident to the domain of analysis have already been deformed due to bathymetric changes in Ω_∞; this history of waves can be described by the mild-slope equation. Therefore, the line-source must be created along the interface Γ between the domain of analysis and the PML, while outgoing waves from the domain of

analysis to Ω_∞ are attenuated in the PML.

If the element mesh consists of linear triangles, denote by (n_i, n_j, n_k) the nodes of an element, a side (n_i, n_j) of which is on the line Γ, $(\zeta_i^G, \zeta_j^G, \zeta_k^G)$ the component of geometric optics, and $\{K_{ijk}\}$ the element's local stiffness matrix for the mild-slope equation, the second domain integral in Eq. (4.7). The line-source is made by supplying the quantities evaluated by

$$\{q_i, q_j\}^T = -2.0\{K_{ijk}\}\{\zeta_i^G, \zeta_j^G, \zeta_k^G\}^T \quad (4.8)$$

to the corresponding nodes in the matrix equation obtained from discretization of Eq. (4.7). The factor 2.0 comes from the fact that elements in both sides of the line ij affect the quantities at the nodes i and j, and the minus sign is due to phase matching.

4.2 *One-dimensional problems*

A. Method 1

The PMLs are set up on both sides of the domain of analysis Ω, in Ω_∞ and $\Omega_{-\infty}$ as shown Fig. 4.2, and it is assumed that waves are incident from the offshore domain Ω_∞. With the similar discussion for the two-dimensional problem above, the weak form for FEM in this case is given as follows (**Appendix**):

$$\int_\Omega \left\{cc_g\nabla\nu_1\nabla\zeta - \nu_1(m\omega)^2\left(\frac{c_g}{c} - \frac{i}{m\omega}f_d\right)\zeta + \nu_1 Q\right\}d\Omega$$
$$+\int_{\Omega_\infty}\left\{\frac{cc_g}{\lambda}\nabla\nu_1\nabla\zeta^\infty - \nu_1(m\omega)^2\left(\frac{c_g}{c} - \frac{i}{m\omega}f_d\right)\lambda\zeta^\infty\right\}d\Omega_\infty$$
$$+\int_{\Omega_{-\infty}}\left\{\frac{cc_g}{\lambda}\nabla\nu_1\nabla\zeta^{-\infty} - \nu_1(m\omega)^2\left(\frac{c_g}{c} - \frac{i}{m\omega}f_d\right)\lambda\zeta^{-\infty}\right\}d\Omega_{-\infty}$$
$$-\left|\nu_1 cc_g B\zeta\right|_{\Gamma_B} - \left|\nu_1 cc_g D\zeta\right|_{\Gamma_D} = 0. \quad (4.9)$$

With the aid of the same approach descried for Eq. (4.7), the point-source can be added at the node between the domain of analysis and the PML. The quantity to be supplied to the node i is given by

$$\{q_i\} = -2.0\{K_{ij}\}\{\zeta_i^G, \zeta_j^G, \cdots\}^T, \quad (4.10)$$

for the linear element, where $\{K_{ij}\}$ is the element's local stiffness matrix in the domain Ω_∞. The factor 2.0 comes from the fact that two elements affect the quantity at the node i, and the minus sign is due to phase matching.

B. Method 2

On the other hand, if the wave field in the offshore domain Ω_∞ is assumed to be linear, the radiative boundary condition can be applied at the end-side of the domain of analysis. Thus the PML is set up only on the transmission side, in $\Omega_{-\infty}$, and then the weak form for FEM is given as follows (**Appendix**):

$$\int_\Omega \left\{cc_g\nabla\nu_1\nabla\zeta - \nu_1(m\omega)^2\left(\frac{c_g}{c} - \frac{i}{m\omega}f_d\right)\zeta + \nu_1 Q\right\}d\Omega$$
$$+\int_{\Omega_{-\infty}}\left\{\frac{cc_g}{\lambda}\nabla\nu_1\nabla\zeta^{-\infty} - \nu_1(m\omega)^2\left(\frac{c_g}{c} - \frac{i}{m\omega}f_d\right)\zeta\lambda^{-\infty}\right\}d\Omega_{-\infty}$$
$$-\left|\nu_1 cc_g B\zeta\right|_{\Gamma_B} - \left|\nu_1 cc_g D\zeta\right|_{\Gamma_D} = \left|\nu_1 cc_g\boldsymbol{n}\cdot\nabla\zeta\right|_\Gamma. \quad (4.11)$$

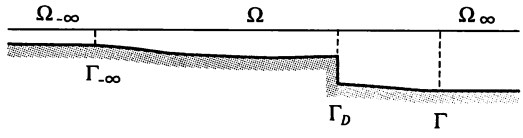

Fig. 4.2. Model definition in one-dimension.

The right-hand side acts as an external force, a source function, specified by the boundary value. Waves in Ω_∞ consist of incident and reflected waves, i.e., $\zeta = \exp(ikx) + \mu\exp(-ikx)$, where μ is the reflection coefficient. Taking differentiation $\nabla\zeta$ and eliminating μ from these two equations gives $\nabla\zeta$. Thus, it follows with $\nu_1 = 1$ that on the line Γ

$$\left|\nu_1 cc_g\boldsymbol{n}\cdot\nabla\zeta\right|_\Gamma = \left|\nu_1 cc_g\nabla\zeta\right|_\Gamma$$
$$= -ikcc_g\zeta + 2ikcc_g\exp(ikx). \quad (4.12)$$

5. Discussions

To exploit the power PML as an absorbing material, we have to specify two of the three PML parameters: the PML thickness D, the scaling parameter β, and the parameter γ for the reflection coefficient for PML-waves. Through numerical experiments for linear and nonlinear wave propagation in one-dimension, the discussion on these unknowns is proceeded to clarify the characteristics of PMLs and, as a result, to show how to design them.

5.1 *Linear wave propagation*

The first issue is wave propagation on water of constant depth, in which the mild-slope equation is implemented with the power PML. The experimental conditions are: the constant water depth is 30 cm, the incident wave period is 1.5 sec, and the length of the domain of analysis is 14 m. This domain is discretized with the linear finite element using 20 nodal points per wavelength L. The incident wave arrives form $x \sim +\infty$. Note that the wave period of 1.3 sec is used in mesh generation to generate a little small size elements. The PML is set up only on the transmission side (Method 2). At the wave incident side, $x = 14$ m, the incident wave is specified as the boundary value problem, and the linear transparent boundary condition for outgoing waves toward $x \sim +\infty$ is applied.

(1) Parameter γ for the reflection of PML-waves

Figure 5.1 shows a comparison of the wave absorption in the PMLs ($m = 0, 1, 2, 4$), where the abscissa is the distance in meters, the ordinate is the dimensionless wave height K relative to the incident wave height, and the left-PML with the thickness of 20 nodal points is set up in the domain $x \leq 0$, i.e. $D \fallingdotseq L$. In this figure, however, the domain $x \leq 4$ is illustrated.

Each figure indicates the effects of the parameter γ on the reflection of PML-waves with constant ($m = 0$), linear

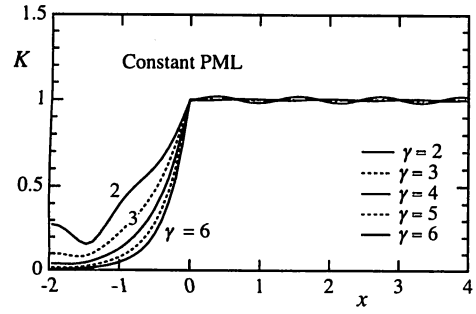

(1) Constant PML (m = 0).

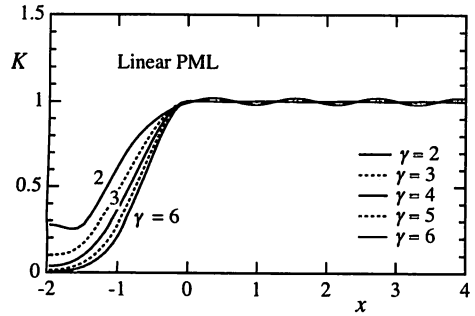

(2) Linear PML (m = 1).

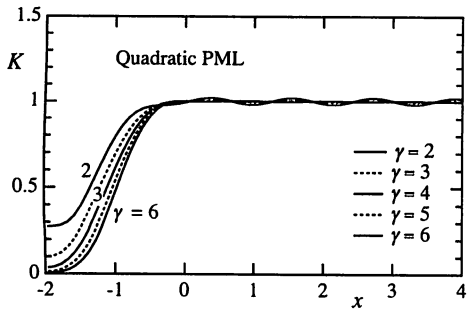

(3) Quadratic PML (m = 2).

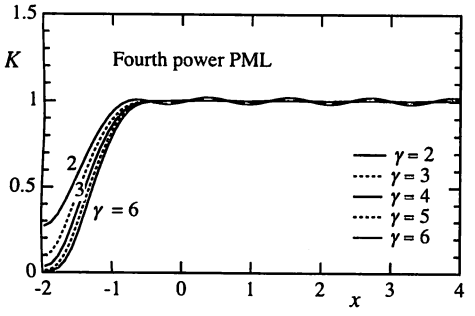

(4) Fourth power PML (m = 4).

Figure 5.1. Wave absorption in the PMLs: $D = L$.

Table 5.1. Outgoing wave heights for various power PMLs.

m	PML	$\gamma = 5$	$\gamma = 6$
0	Constant	0.014	0.0051
1	Linear	0.014	0.0050
2	Quadratic	0.013	0.0047
4	Fourth power	0.012	0.0040
5	Fifth power	0.011	0.0035

(m = 1), quadratic (m = 2), and fourth power (m = 4) attenuation functions. The values of γ from 2 to 6 with an interval of 1 are examined. Note that the exact solution in the domain $x \geq 0$ is unity, i.e., $K = 1$.

Among the PMLs, the constant PML may be sensitive to the reflection of discretization-waves at the interface $x = 0$ between the PML and the domain of analysis because of a sudden decrease in wave heights. To make this reflection small, the absorption of waves in the PML has to be turned on gradually and smoothly; the constant PML cannot achieve this.

A common property in these PMLs is the reflection of PML-waves for $\gamma = 2$, i.e., resulting ripples propagate toward $x \sim +\infty$. For large values of γ, the PMLs except the constant PML gradually absorb waves near the interface at $x = 0$ and then sharply absorb waves on the way to the end-side of the PML. Increase in γ makes the PMLs effective.

Table 5.1 gives the outgoing wave heights at the end-side of various power PMLs, resulting form the numerical experiments. Since the outgoing wave at the end-side of PML is given, from Eq. (3.33) in the present case, by

$$\zeta \fallingdotseq \exp(-\gamma)\exp(-ikR_p), \quad x = -R_p, \qquad (5.1)$$

the outgoing wave height is approximated theoretically by $K \sim 2\exp(-\gamma)$. Since $\exp(-5) \fallingdotseq 0.0067$ and $\exp(-6) \fallingdotseq 0.0025$, the numerical results given in Table 4.1 agree well with the theoretical ones. In the PMLs for $m \leq 2$ with $\gamma = 6$, the outgoing wave height is about 0.5% of the incident wave height; i.e., the reflection of PML-waves is about 0.5%. The higher order power PMLs for $m > 2$ absorb outgoing waves more gradually near the interface at $x = 0$, and the reflection of PML-waves becomes small enough. Consequently, in the following discussions, the quadratic PML with the parameter $\gamma = 6$ is exploited as a wave absorber, along with the prevention of the reflection of discretization-waves.

(2) PML thickness

Figure 5.2 shows the effect of the PML thickness on wave absorbing properties, where the PML thickness is $D = L/2$. In Fig. 5.2 (1), the number of nodes in the PML is 10 points, and the element size is $L/20$, the same as in Fig. 5.1. In Fig. 5.2 (2), the number of nodes is 20 points, and thus the element size is $L/40$.

Since the PML thickness is the half of that used in Fig. 5.1, the wave entering into the PML has to decay much quicker than that in Fig. 5.1 (3). The wave attenuation in the PML with 10 nodal points is not enough because disagreeable ripples due to the PML-waves appear in the domain $x \geq 0$; the reason is the lack of nodal points in the PML. On the contrary, the PML with 20 nodal points attenuates accurately the wave.

Generally, if the PML thickness becomes narrow, the decay of waves is so rapid that many nodal points in the PML are needed to simulate accurately the wave decaying

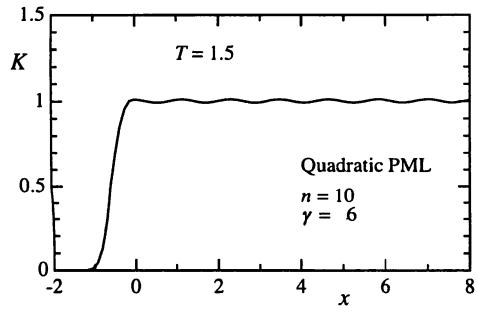

(1) Using 10 nodal points in the PML.

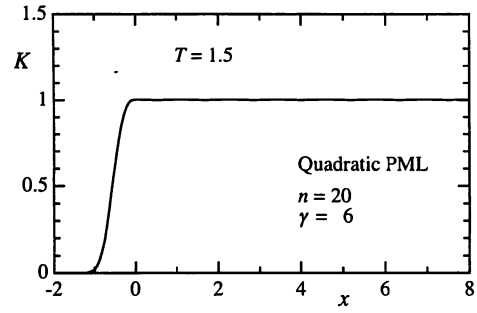

(2) Using 20 nodal points in the PML.

Figure 5.2. Effects of the PML thickness and the number of nodes on wave absorption: $D = L/2$.

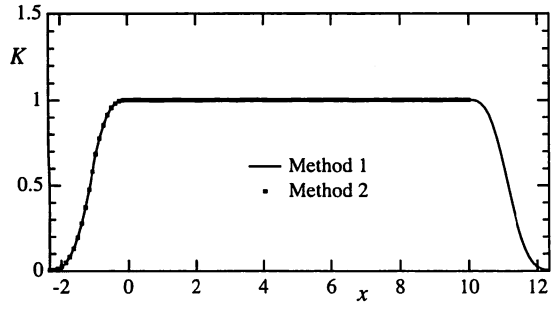

Figure 5.3. Comparison of the methods for incident conditions: $D = 2L$.

property. Consequently, there may be no benefit to make the PML thickness narrow; the matter of considerable significance in design of the PML is the number of nodal points in the PML.

(3) Methods for incident wave conditions

So far, the PML is set up only on the transmission side (Method 2). Method 1 is the case where the PMLs are set up on both the incident and transmission sides of the domain of analysis. Figure 5.3 compares these methods to evaluate their ability of outgoing wave absorption and to examine the approaches for source function setting. The experimental conditions are: the constant water depth is 30 cm, the incident wave period is 1.5 sec, the length of the domain of analysis is 10 m ($0 \leq x \leq 10$) with the linear finite element using 20 nodal points per wavelength L, the PMLs are in the regions $x < 0$ and $x > 10$, and the PML thickness is $D = 2L$; it is enough length to remove the effects of discretization-waves on the numerical results.

The results obtained from these two methods coincide with in the computational region of interest. This shows the ability of Method 2 and the validity of Method 1 if the incident side domain is assumed to be linear.

5.2 *Nonlinear wave propagation*

The second issue is nonlinear wave propagation, in which higher harmonics appear due to the nonlinear interaction. The model wave equation is an infinite set of coupled nonlinear partial differential equations for all harmonics (**Appendix**). Therefore, the PML must absorb all the target harmonics.

Consider an example of nonlinear wave propagation on a step-type reef, without wave breaking, as shown in the bottom of Fig. 5.4, where the abscissa is the distance in meters. The bathymetric conditions are: the water depth in the offshore domain ($10 < x \leq 16$) is $h_1 = 37.5$ cm, the water depth on the reef flat ($x < 10$) is $h_2 = 7.5$ cm, and the water depth ratio is $\delta = h_2/h_1 = 0.2$. In this figure, however, the domain $x \leq 14$ is illustrated.

The incident wave arrives from $x \sim +\infty$, the deeper side of the step, the incident wave period is $T = 1.02$ sec, and the amplitude is $a_0 = 1.1$ cm. The offshore domain is assumed to be a linear because of $T(g/h_2)^{1/2} = 5.21$, and the domain on the reef flat be a nonlinear because of $T(g/h_2)^{1/2} = 11.7$. The element size in the offshore domain is 1/20 of the wavelength L for an incident wave. Although must be specified based on higher harmonics and properties of the problem, in this case, the element size on the reef flat is decided as 1/20 of the wavelength evaluated using the incident wave period.

The quadratic left-PMLs with the thickness L and $2L$ are set up only in the domain $x \leq 0$ (Method 2). The PML parameter for the reflection coefficient is $\gamma = 6$, and the element size in the PMLs is the same as that on the reef flat. At the wave incident side, $x = 16$ m, the incident wave is specified as the boundary value problem, and the linear transparent boundary condition for outgoing waves toward $x \sim +\infty$ is applied. The PML equation is derived from the complex coordinate stretching of the mild-slope equation, the same as the linear parts of the governing equation; this means that the PML equation is applied separately to each harmonic. It is assumed here that the number of harmonics is five, i.e., $M = 5$.

To investigate the effects of PML thickness upon the ability of absorption for nonlinear waves, Fig. 5.4 shows the distribution of dimensionless amplitudes for the first five harmonics $|\zeta_m|$ ($m = 1, 2, \cdots, 5$) and the wave height K, in which the local wave height is defined as a crest to trough height. Differences of the distribution of amplitudes and the wave height for $x > 0$ between the results for the PML thickness $D/L = 1$ (solid lines) and for $D/L = 2$ (broken lines) are hardly visible in the figure; they distribute smoothly on the reef flat ($0 \leq x \leq 10$) and are thus acceptable. Theoretical results are fairly agree with

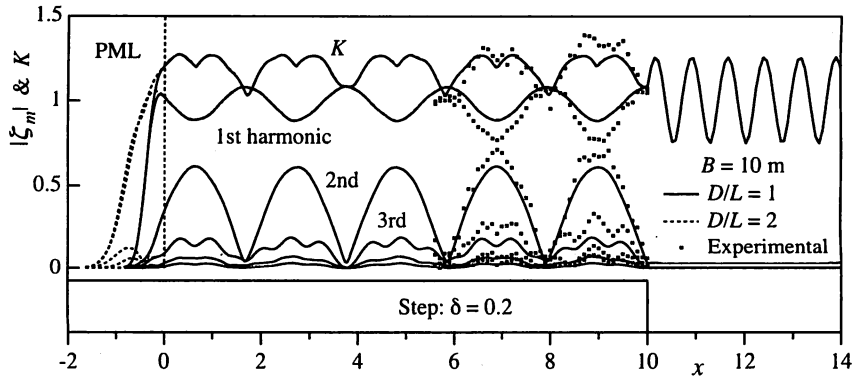

Fig. 5.4. Distribution of amplitudes of harmonics on the step-type reef: D/L = 1 and 2.

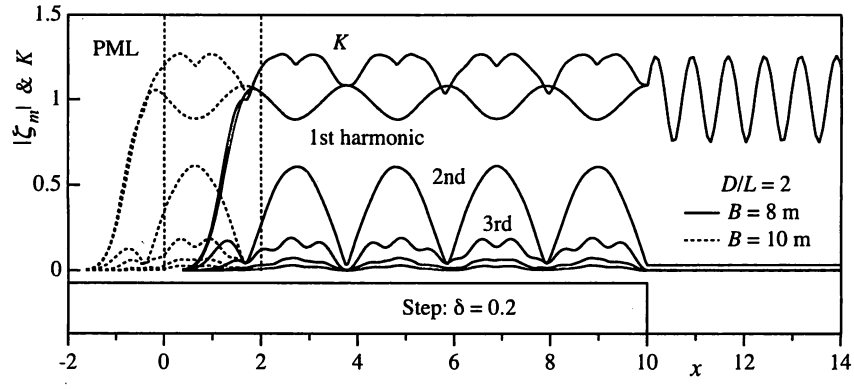

Fig. 5.5. Distribution of amplitudes of harmonics on the step-type reef: B = 10 and 12 m.

the experimental ones, denoted by the dots (Ohki, 1997).

The outgoing wave heights at the end-side of the PML are $K \fallingdotseq 0.0059$ and 0.0066 for $D/L = 1$ and $D/L = 2$, respectively. Probably because of nonlinearlity of waves on the reef flat, these values are a little larger than the wave height $K = 0.005$ designed for each harmonic, but the total reflection of PML-waves is about 0.6-0.7% of the incident wave height; therefore, it is small enough.

Similarly, two widths of the domain of analysis, 8 and 10 m on the reef flat, are examined to evaluate the reflection of discretization-waves. As shown in Fig. 5.5, the PML with $D/L = 2$ is set up on the transmission side (Method 2). Both distributions of the amplitude for harmonics and the wave height coincide for $x \geq 2$; this indicates that there is no reflection of discretization-waves at the interface between the PML and the domain of analysis.

The result discussed above implies the ability and efficiency of the PMLs for outgoing wave absorption. The efficient PML requires (1) gradual wave absorption near the interface between the PML and the domain of analysis and (2) enough nodal points to follow accurately quick decay in wave heights. The PML with a wide thickness is effective to both requirements: gradual wave absorption, which also diminishes discretization-waves, and enough nodal points with the same element size as in the domain of analysis. An approach to the second requirement is to use smaller elements in the PML than that in the domain of analysis, as was the case in Fig. 5.2 (2).

A typical PML thickness is one or two times the wavelength for an incident wave, as was used in obtaining the finite difference solutions to nonlinear water wave propagation problems (e.g., Gobbi and Kirby, 1999), in which the thickness of the absorbing materiel is two times the wavelength.

6. Concluding Remarks

The perfectly matched layer, especially the power PML, is effective and easy to exploit as an absorbing material for linear and nonlinear waves with arbitrary frequencies. The model wave equation implemented for nonlinear wave-deformation problems is convenient to introduce the PML because the linear terms are identical to the mild-slope equation; the PML methodology has to apply to the linear wave equation. In nonlinear wave propagation problems, it is significant to absorb gradually each harmonic in the PML with the wide thickness and enough nodal points.

The PML equation for multidimensional problems is derived by the independent complex coordinate stretching, the same way as in one-dimensional problems. Therefore, characteristics of the one-dimensional PML is especially significant in design of PMLs.

As a result of numerical experiments for water wave

propagation in one-dimension, based on the FEM, the PML available as a nonlinear wave absorber can be designed as follow.

(1) The use of the quadratic PML or higher order power PMLs is recommended.
(2) The parameter for the reflection coefficient for PML-waves is $\gamma = 6$ or a little larger value.
(3) The PML thickness D for the linear wave analysis is nearly equal to the wavelength for an incident wave, and the element size is 1/20 of the wavelength.
(4) The PML thickness D for the nonlinear wave analysis is equal to or two times the wavelength for an incident wave, and the element size must be specified taking account of the wavelength for higher harmonics.
(5) The scaling parameter is specified by $\beta = \gamma/D$.

References

Abohadima, S., Yu, X., and Isobe, M. (1999): Numerical calculation of wave diffraction by nonlinear mild-slope equations, *Proc. Coastal Eng.*, JSCE, 46, pp.51-55 (in Japanese).

Arikawa, T. and Isobe, M. (1999): Numerical simulation of stem waves along wave-dissipating breakwater with nonlinear mild-slope equations, *Proc. Coastal Eng.*, JSCE, 46, pp.56-60 (in Japanese).

Bérenger, J. -P. (1994): A perfectly matched layer for the absorption of electromagnetic waves, *Jour. of Compu. Physics*, 114 (2), pp.185-200.

Bermúdez, A., Hervella-Nieto, L., Prieto, A., and Rodríguez, R. (2004): An exact bounded PML for the Helmholtz equation. *C. R. Acad. Sci. Paris, Series I*, 339, pp.803-808.

Bettess, P., Emson, C., and Chiam, T. C. (1984): A new mapped infinite element for exterior wave problems, *Numerical Methods in Coupled Systems*, eds. R. W. Lewis *et al.* (John Wiley & Sons Ltd.), pp.489-504.

Bindel, D. S. and Govindjee, S. (2005): Elastic PMLs for resonator anchor loss simulation, *Bull. Dep. of Civil and Environ. Eng.*, Univ. of California, Berkeley, Report No. UCB / SEMM-2005/01, 24pp.

Chadwick, E., Bettess, P., and Laghrouche, O. (1999): Diffraction of short waves modelled using new mapped wave envelope finite and infinite elements, *Int. Jour. Num. Meth. Eng.*, 45, pp.335-354.

Chen, H. S. and C. C. Mei (1975): Hybrid-element method for water waves, *Proc. Modelling Techniques Conf. (Modelling 1975)*, 1, pp.63-81.

Chen, H. S. (1990): Infinite elements for water wave radiation and scattering, *Int. Jour. Num. Meth. Fluid*, 11, pp.555-569.

Chew, W. C. and Weedon, W. H. (1994): A 3d perfectly matched medium from modified Maxwell's equations with stretched coordinates, *Microwave and Optical Techno. Lett.*, 7 (13), pp.599-604.

Cruz, E. C., Yokoki, H., Isobe, M., and Watanabe, A. (1993): Nonreflecting boundary conditions for nonlinear wave equations, *Proc. Coastal Eng.*, JSCE, 40, pp.46-50 (in Japanese).

Cruz, E. C., Ishikura, M., and Aono, T. (1997): Simulation of nonlinear dispersive wave evolution in open-bounded domains, *Proc. Coastal Eng.*, JSCE, 44, pp.46-50 (in Japanese).

Dalrymple, R. A., J. T. Kirby and P. A. Hwang (1984): Wave diffraction due to areas of energy dissipation, *Jour. Waterway, Port, Coastal, and Ocean Eng.*, ASCE, 110, pp.67-79.

Gobbi, M. F. and Kirby, J. T. (1999): Wave evolution over submerged sills: tests of a high-order Boussinesq model, *Coastal Engineering*, 37, pp.57–96.

Ishii, T., Isobe, M., and Watanabe, A. (1994): Improved boundary conditions to a time-dependent mild-slope equation for random waves, *24th Inter. Conf. on Coastal Eng.*, ASCE, 1, pp.272-284.

Izumiya, T. and K. Horikawa (1984): Wave energy equation applicable in and outside the surf zone, *Coastal Eng. in Japan*, JSCE, 27, pp.119-137.

Johnson, S. G., Bienstman, P., Skorobogatiy, M., Ibanescu, M., Lidorikis, E., and Joannopoulos, J. D. (2002): Adiabatic theorem and continuous coupled-mode theory for efficient taper transitions in photonic crystals, *Phys. Rev. E.*, 66, p.066608.

Kiyokawa, S., Nadaoka, K., Beji, S. (1996): An approach for open boundary treatment in simulation of nonlinear wave propagation, *Proc. Coastal Eng.*, JSCE, 43, pp.6-10. (in Japanese).

Kubo, T., Kotake, Y., Yokoki, H., Isobe, M., and Watanabe, A. (1992): Prediction model for the fields of waves, nearshore current, and beach deformation base on a time-dependent mild-slope equation for random waves, *Proc. Coastal Eng.*, JSCE, 39, pp.201-205 (in Japanese).

Larsen, J. and Dancy, H. (1983): Open boundaries in short wave simulations - A new approach, *Coastal Eng.*, 7, pp. 285-297.

Lee, C. and Yoon, S. B. (2004): Effect of higher-order bottom variation terms on the refraction of water waves in the extended mild-slope equations, *Coastal Eng.*, 31, pp.865-882.

Mesquit, E. and Pavanello, R. (2005): Numerical methods for the dynamics of unbounded domains, *Compu. & Applied Math.*, 24 (1), pp. 1-26.

Navon, I. M., Neta, B., and Hussaini, M. Y. (2004): A Perfectly matched layer approach to the linearized shallow water equations models, *Monthly Weather Review*, AMS, 132, pp.1369-1378.

Ohki, H. (1997): Evolution of Nonlinear Dispersive Waves on the Reef Coast and Wave Height Distribution, *Master Thesis in Civil Eng. and Archi.*, Graduate School of Eng., Univ. of the Ryukyus, 64pp (in Japanese).

Ohyama, I. and Nadaoka, K. (1990): Development of a numerical absorbing filter for open boundary treatment in the numerical wave-flume, *Proc. Coastal Eng.*, JSCE, 37, pp.16-20 (in Japanese).

Park, W.-S., Yun, C.-B., and Pyun, C.-K. (1991): Infinite elements for evaluation of hydrodynamic force on offshore structures, *Computer & Structures*, 40 (4), pp.837-847.

Sacks, Z. S., Kingsland, D. M., Lee, R., and Lee, J.-F. (1995): A perfectly matched anisotropic absorber for use as an absorbing boundary condition, *IEEE Trans. Antennas and Propagation*, 43 (12), pp.1460-1463.

Sato, N., Isobe, M., and Izumiya, T. (1988): Improved numerical method of wave height distribution for random waves in the harbor of arbitrary shape, *Proc. Coastal Eng.*, JSCE, 35, pp.257-261. (in Japanese).

Sulaiman, D. M ., S. Tsutsui, H. Yoshioka, S. Oshiro, and Y. Tsuchiya (1994): Prediction of the maximum wave on the coral flat, *Proc. 24th Inter. Conf. on Coastal Eng.*, ASCE, pp.6.9-6.23.

Teixeira, F. L. and Chew, W. C. (1997): PML-FDTD in Cylindrical and Spherical Grids, *Microwave and Guided Wave Lett.*, 7 (9), pp.285-287.

Teixeira, F. L. and Chew, W.C. (2000): Finite-difference computation of transient electromagnetic waves for cylindrical geometries in complex media, *IEEE Transactions on Geoscience and Remote Sensing*, 38, (4). pp.1530-1543.

Turkel, E. (1998): Introduction to the special issue on absorbing boundary conditions, *Applied Num. Math.*, 27 (4), pp.327-329.

Turkel, E. and Yefet, A. (1998): Absorbing PML boundary layers for wave-like equations, *Applied Num. Math.*, 27 (4), pp. 533-557.

Tsutsui, S. and D. P. Lewis (1992): Wave height prediction in unbounded coastal domains with bathymetric discontinuity, *Coastal Eng. in Japan*, JSCE, 34, pp.145-158.

Tsutsui, S. and K. Zamami (1993): Jump condition of energy flux at the line of bathymetric discontinuity and wave breaking on the reef flat, *Coastal Eng. in Japan*, JSCE, 36, pp.155-175.

Tsutsui, S., Suzuyama, K., and Ohki, H. (1996): Model equations of nonlinear dispersive waves in shallow water and its application to the step-type reef, *Proc. Coastal Eng.*, JSCE, 43, pp.16-20 (in Japanese).

Tsutsui, S., Suzuyama, K., and Ohki, H. (1998): Model equations of nonlinear dispersive waves in shallow water and an application of its simplified version to wave evolution on the step-type reef, *Coastal Eng. Jour.*, JSCE, 40 (1), pp.41-60.

Tsutsui, S. and Ohki, H. (1998): Nonlinear wave evolution on the slope-

and step-type reefs, *Proc. Coastal Eng.*, JSCE, 45, pp.41-45 (in Japanese).

Tsutsui, S. (2003): Coastal wave-deformation models combined with integrable-type infinite elements, *Coastal Eng. Jour.*, JSCE, 45 (1), pp.83-118.

Wei, G. and Kirby, J. T., (1995): Time-dependent numerical code for extended Boussinesq equations. *Jour. Waterway, Port, Coast., Ocean Eng.*, ASCE, 121, pp.251-261.

Yamashita, T., Y. Tsuchiya, M. Matsuyama and T. Suzuki (1990): Numerical calculation of linear wave propagation in the coastal zone, *Bull. Disas. Prev. Res. Inst.*, Kyoto Univ., 40, pp.15-40.

Yu, X. (1998): One-way wave equation as non-reflecting boundary conditions, *Proc. Coastal Eng.*, JSCE, 45, pp.31-35 (in Japanese).

Zeng, Y. Q., He, J. Q., and Liu, Q. H. (2001): The application of the perfectly matched layer in numerical modeling of wave propagation in poroelastic media, *Geophysics*, 66 (4), pp. 1258 - 1266,.

Zienkiewicz, O. C., Bando, K., Bettess, P., Emson, C., and Chian, T. C. (1985): Mapped infinite elements for exterior wave problems, *Int. Jour. for Num. Methods in Eng.*, 21, pp.1229-1251.

Appendix. Governing Equations, Boundary conditions, and Weak Form for FEM

1. Governing Equation

1.1 *Model wave equation*

The nonlinear wave-deformation model implemented in CATWAVES (Tsutsui *et al.*, 1996, 1998; Tsutsui and Ohki, 1998; Tsutsui, 2003) is described. The physical variables are non-dimentionalized by the representative length h_0^*, the time $(h_0^*/g)^{1/2}$, and the velocity $(gh_0^*)^{1/2}$, where h_0^* is a constant water depth, g is the acceleration of gravity, and the asterisk (*) denotes dimensional variables.

Denote by (x^*,y^*) the horizontal coordinates, where the coordinate origin being on the still water level, h^* the local water depth, η^* the free surface displacement, and a_0^* the incident wave amplitude, ω^* the frequency, k^* the wave number, c^* the wave velocity, and c_g^* the group velocity. The dimensionless variables are then defined as:

$$\left.\begin{array}{c}(x,y,h,\eta,a_0)=(x^*,y^*,h^*,\eta^*,a_0^*)/h_0^* \\ \omega=\omega^*\sqrt{h_0^*/g},\quad k=k^*h_0^* \\ (c,c_g)=(c^*,c_g^*)/\sqrt{gh_0^*}\end{array}\right\}. \qquad (A.1)$$

Assume that the free surface displacement can be expressed as the Fourier series:

$$\eta(x,y,t)=\frac{1}{2}\sum_m \eta_m(x,y)\exp(-im\omega t), \qquad (A.2)$$

with $m=\pm1,\pm2,\cdots$, where $i=(-1)^{1/2}$ is the imaginary unit and η_{-m} is the complex conjugate of η_m. The model wave equation for the m-th harmonic of the Fourier components is given by

$$\begin{aligned}&\frac{\partial}{\partial x}\left(cc_g\frac{\partial\zeta_m}{\partial x}\right)+\frac{\partial}{\partial y}\left(cc_g\frac{\partial\zeta_m}{\partial y}\right)+(m\omega)^2\left(\frac{c_g}{c}-\frac{i}{n\omega}f_d\right)\zeta_m \\ &=\frac{\varepsilon}{2}\sum_{l=-\infty}^{\infty}(m^2-l^2)\omega^2\frac{c_g}{c}\zeta_l\zeta_{m-l} \\ &-\frac{\varepsilon}{2}\sum_{l=-\infty,\,l\neq n}^{\infty}\frac{m+l}{m-l}cc_g\left(\frac{\partial\zeta_l}{\partial x}\frac{\partial\zeta_{m-l}}{\partial x}+\frac{\partial\zeta_l}{\partial y}\frac{\partial\zeta_{m-l}}{\partial y}\right) \\ &-\frac{\varepsilon}{2}\sum_{l=-\infty,\,l\neq m}^{\infty}\frac{2}{l(m-l)\omega^2}c^3c_g \\ &\times\left(\frac{\partial^2\zeta_l}{\partial x^2}\frac{\partial^2\zeta_{m-l}}{\partial y^2}-\frac{\partial^2\zeta_l}{\partial x\partial y}\frac{\partial^2\zeta_{m-l}}{\partial x\partial y}\right), \qquad (A.3.1)\end{aligned}$$

with $l=\pm1,\pm2,\cdots$ and

$$\left.\begin{array}{l}\zeta_m=\dfrac{\eta_m}{a_0},\quad \varepsilon=\dfrac{a_0}{h} \\ c^2=\dfrac{1}{k}\tanh kh,\quad \dfrac{c_g}{c}=\dfrac{1}{2}\left(1+\dfrac{2kh}{\sinh 2kh}\right)\end{array}\right\}. \qquad (A.3.2)$$

In the equation (A.3), the energy dissipation by wave breaking (Dalrymple, *et al.*, 1984) and bottom friction is taken account of in the coefficient f_d, and the physical quantities: the frequency ω, the wave number k, the wave velocity c, and the group velocity c_g, are the values for the m-th harmonic.

Equation (A.3) is an infinite set of coupled nonlinear partial differential equations for all harmonics. If the nonlinearlity is weak, the significance of higher harmonics diminishes with increase in the Fourier modes. We can therefore truncate the Fourier series after a finite number of terms (say M) and solve the M sets of equations for the M unknown free surface displacement with well-posed boundary conditions.

For the maximum number of Fourier modes, M, the nonlinear terms Q in the model wave equation can be modified as follows:

$$\begin{aligned}Q=&\sum_{l=1}^{m-1}A_{1,l}\zeta_{m-l}+\sum_{l=1}^{M-m}A_{2,-l}\zeta_{m+l} \\ &+\sum_{l=1}^{m-1}\left(B_{1,l}\frac{\partial\zeta_{m-l}}{\partial x}+B_{2,l}\frac{\partial\zeta_{m-l}}{\partial y}\right) \\ &+\sum_{l=1}^{m-1}\left(B_{1,l}\frac{\partial\zeta_{m-l}}{\partial x}+B_{2,l}\frac{\partial\zeta_{m-l}}{\partial y}\right) \\ &+\sum_{l=1}^{M-m}\left(B_{3,-l}\frac{\partial\zeta_{m+l}}{\partial x}+B_{4,-l}\frac{\partial\zeta_{m+l}}{\partial y}\right) \\ &+\sum_{l=1}^{m-1}\left(C_{1,l}\frac{\partial^2\zeta_{m-l}}{\partial y^2}+C_{2,l}\frac{\partial^2\zeta_{m-l}}{\partial x\partial y}\right) \\ &+\sum_{l=1}^{M-m}\left(C_{3,-l}\frac{\partial^2\zeta_{m+l}}{\partial y^2}+C_{4,-l}\frac{\partial^2\zeta_{m+l}}{\partial x\partial y}\right), \qquad (A.4)\end{aligned}$$

with

$$\left.\begin{array}{l}A_{1,l}=\dfrac{\varepsilon}{2}(m^2-l^2)\omega^2\dfrac{c_g}{c}\zeta_l \\ A_{2,-l}=\dfrac{\varepsilon}{2}(m^2-2ml-2l^2)\omega^2\dfrac{c_g}{c}\zeta_{-l} \\ A_{2,-l}=\dfrac{\varepsilon}{2}(m^2-2ml-2l^2)\omega^2\dfrac{c_g}{c}\zeta_{-l}\end{array}\right\}, \qquad (A.5.1)$$

$$\left.\begin{array}{l}B_{1,l}=-\dfrac{\varepsilon}{2}\dfrac{m+l}{m-l}cc_g\dfrac{\partial\zeta_l}{\partial x} \\ B_{2,l}=-\dfrac{\varepsilon}{2}\dfrac{m+l}{m-l}cc_g\dfrac{\partial\zeta_l}{\partial y} \\ B_{3,-l}=\varepsilon\left(\dfrac{l}{m+l}+\dfrac{m}{l}\right)cc_g\dfrac{\partial\zeta_{-l}}{\partial x} \\ B_{4,-l}=\varepsilon\left(\dfrac{l}{m+l}+\dfrac{m}{l}\right)cc_g\dfrac{\partial\zeta_{-l}}{\partial y}\end{array}\right\}, \qquad (A.5.2)$$

$$\left.\begin{aligned} C_{1,l} &= -\varepsilon \frac{c^2}{l(m-l)\omega^2} cc_g \frac{\partial^2 \zeta_l}{\partial x^2} \\ C_{2,l} &= +\varepsilon \frac{c^2}{l(m-l)\omega^2} cc_g \frac{\partial^2 \zeta_l}{\partial x \partial y} \\ C_{3,-l} &= +\varepsilon \frac{2c^2}{l(m+l)\omega^2} cc_g \frac{\partial^2 \zeta_{-l}}{\partial x^2} \\ C_{4,-l} &= -\varepsilon \frac{2c^2}{l(m+l)\omega^2} cc_g \frac{\partial^2 \zeta_{-l}}{\partial x \partial y} \end{aligned}\right\}, \quad \text{(A.5.3)}$$

where the subscripts $\pm l$ for A_k, B_k, and C_k indicate that these are functions of $\zeta_{\pm l}$.

When all the nonlinear terms in the right-hand side of Eq. (A.3) are neglected, the model wave equation reduces to the mild-slope equation with energy dissipation:

$$\frac{\partial}{\partial x}\left(cc_g \frac{\partial \zeta_m}{\partial x}\right) + \frac{\partial}{\partial y}\left(cc_g \frac{\partial \zeta_m}{\partial y}\right) + (m\omega)^2\left(\frac{c_g}{c} - \frac{i}{n\omega} f_d\right)\zeta_m = 0. \quad \text{(A.6)}$$

Therefore, the finite element approximation based on the model wave equation (A.3), a variant of the mild-slope equation, covers both linear and nonlinear wave motion.

The complex coordinate stretching for the PML can be applied only to the linear parts of the wave equation, i.e., Eq. (A.6). With the aid of Eq. (2.15), the PML equation is given by

$$\frac{1}{\lambda_1}\frac{\partial}{\partial x}\left(cc_g \frac{1}{\lambda_1}\frac{\partial \zeta_m}{\partial x}\right) + \frac{1}{\lambda_2}\frac{\partial}{\partial y}\left(cc_g \frac{1}{\lambda_2}\frac{\partial \zeta_m}{\partial y}\right) + (m\omega)^2\left(\frac{c_g}{c} - \frac{i}{n\omega} f_d\right)\zeta_m = 0. \quad \text{(A.7.1)}$$

Multiplying Eq. (A.7.1) by $\lambda_1(x)\lambda_2(y)$ results in

$$\frac{\partial}{\partial x}\left(cc_g \frac{\lambda_2}{\lambda_1}\frac{\partial \zeta_m}{\partial x}\right) + \frac{\partial}{\partial y}\left(cc_g \frac{\lambda_1}{\lambda_2}\frac{\partial \zeta_m}{\partial y}\right) + (m\omega)^2\left(\frac{c_g}{c} - \frac{i}{n\omega} f_d\right)\lambda_1\lambda_2\zeta_m = 0. \quad \text{(A.7.2)}$$

1.2 *Boundary conditions*

The domain of wave analysis is subdivided into two domains, Ω and Ω_∞, by the boundary Γ, as shown in Fig. 4.1. The infinite domain Ω_∞ surrounds the domain Ω and expands to infinity. To release the simplifications of a constant water depth in the far-field, the domain Ω_∞ is further truncated by using the perfectly matched layer (PML) with a finite width. Waves in Ω are governed by the model wave equation (A.3) and waves in the PML by the PML equation. Further, the boundary Γ_B and the lines of water depth discontinuity Γ_D are considered in the domain Ω.

The boundary conditions are therefore as follows: Note that, hereafter, the subscript m for ζ is omitted for brevity.

(1) Continuity condition through the boundary Γ:

$$\zeta = \zeta_\infty, \quad \boldsymbol{n}\cdot\nabla\zeta + \boldsymbol{n}_\infty\cdot\nabla\zeta_\infty = 0, \quad \text{(A.8)}$$

where $\nabla \equiv (\partial/\partial x, \partial/xy)$, ζ and ζ_∞ are the free surface displacement in Ω and Ω_∞, and vectors $\boldsymbol{n}$ and $\boldsymbol{n}_\infty$ are the outward normal from Ω and Ω_∞.

(2) Reflective condition along the boundary Γ_B (Tsutsui and Lewis, 1992):

$$\left.\begin{aligned} &\boldsymbol{n}_B\cdot\nabla\zeta = B\zeta \\ &B = k\left(-i\alpha + \frac{\tanh kh}{1+\cosh kh}\frac{\partial h}{\partial n_B}\right) \\ &\alpha = \frac{1-R}{1+R}\sin\beta_b \end{aligned}\right\}, \quad \text{(A.9)}$$

where the vector $\boldsymbol{n}_B$ is the outward normal to the reflective boundary, α is a real, dimensionless dumping coefficient, R is the reflection coefficient, and β_b is an incident angle to the reflective boundary. The total reflection is given by $\alpha = 0$, the total absorption by $\alpha = 1$, and $0 < \alpha < 1$ for any partial reflection.

(3) Conservation of energy flux at the line of depth discontinuity Γ_D (Tsutsui and Zamami, 1993):

$$\left.\begin{aligned} &\left[cc_g\boldsymbol{n}_D\cdot\nabla\zeta\right]_{\xi_0^-}^{\xi_0^+} = D\zeta \\ &D = \tilde{\gamma}\, h_s(h_d - h_s)\left|\frac{k^2}{\cosh^2 kh}\right|_{\xi_0} \end{aligned}\right\}, \quad \text{(A.10)}$$

where the vector $\boldsymbol{n}_D$ is the outward normal to the line of bathymetric discontinuity ξ_0, along which the coefficient $\tilde{\gamma}$ is specified, and water depths at the deeper and shallower sides are denoted by h_d and h_s, respectively. It is assumed in Eq. (A.10) that waves approach from a deeper to shallower side.

(4) Energy dissipation due to breaking and bottom friction:

The experimental formula of the coefficient of energy dissipation presented by Izumiya and Horikawa (1984) is adopted and it can be approximated by

$$f_d = \left[\frac{1}{2}C_f + \frac{\beta_0}{8}\sqrt{\left(\frac{H}{h}\right)^2 - \left(\frac{H}{h}\right)_s^2}\right]\frac{H}{h}\frac{c_g}{h}, \quad \text{(A.11)}$$

where C_f is the dimensionless coefficient of bottom friction, β_0 the coefficient related with energy dissipation due to wave breaking, H the local wave height, h the still water depth, and $(H/h)_s$ the relative minimum wave height in the surf zone. The energy dissipation due to wave breaking can be applied only if the square root is a real number. The estimated empirical values of coefficients for the slope of 1/20 are $\beta_0 = 1.8$ and $(H/h)_s^2 = 0.72$.

The same expression with Eq. (A.11) have been applied to wave breaking at the tip of the reef (Sulaiman, *et al.*, 1994). The empirical formula for the coefficient β_0 are given as follows:

(a) For the step-type reef

$$\beta_0 = 4.88\exp(-0.0921T) + 0.12, \quad \text{(A.12.1)}$$

(b) For the slope-type reef

$$\left.\begin{aligned} \beta_0 &= 3.27\exp(-0.1027\,T) + 1.73 \quad \text{for } s = 1/20 \\ \beta_0 &= 4.26\exp(-0.0896\,T) + 0.74 \quad \text{for } s = 1/10 \end{aligned}\right\} \quad \text{(A.12.2)}$$

where $T = T^*\sqrt{g/h_r^*}$, h_r^* is the water depth on the reef flat, and s is the slope in front of the reef.

2. Weak form for FEM

2.1 *Two-dimensional problems*

The governing equations and the boundary conditions are summed up as follows:

$$\nabla\cdot(cc_g\nabla\zeta)+(m\omega)^2\left(\frac{c_g}{c}-i\tilde{f}_d\right)\zeta=Q \quad \text{in } \Omega, \tag{A.13}$$

$$\nabla_1\left(\frac{\lambda_2}{\lambda_1}cc_g\nabla_1\zeta^\infty\right)+\nabla_2\left(\frac{\lambda_1}{\lambda_2}cc_g\nabla_2\zeta^\infty\right)+(m\omega)^2\left(\frac{c_g}{c}-i\tilde{f}_d\right)\lambda_1\lambda_2\zeta^\infty=0 \quad \text{in } \Omega_\infty, \tag{A.14}$$

$$\zeta=\zeta^\infty,\quad \boldsymbol{n}\cdot\nabla\zeta+\boldsymbol{n}_\infty\cdot\nabla\zeta^\infty=0 \quad \text{on } \Gamma, \tag{A.15}$$

$$\boldsymbol{n}_B\cdot\nabla\zeta=B\zeta \quad \text{on } \Gamma_B, \tag{A.16}$$

$$[cc_g\boldsymbol{n}_D\cdot\nabla\zeta]_{\xi_0^-}^{\xi_0^+}=D\zeta \quad \text{on } \Gamma_D, \tag{A.17}$$

Sommerfeld's radiation condition at infinity. (A.18)

In Eqs. (A.13) and (A.14), $\tilde{f}_d=f_d/(m\omega)$ for brevity. Equation (A.14) with $(\nabla_1,\nabla_2)=(\partial/\partial x,\partial/\partial y)$ is the PML equation (A.7.2) for the mild-slope equation in Ω_∞. At the interface Γ between the PML and the domain of analysis, both λ_1 and λ_2 take the value unity, and then Eq. (A.14) is identical to the mild-slope equation.

We construct the weak form for FEM to the system of governing equations and boundary conditions, (A.13)-(A.17); Eq. (A.18) is be satisfied in implementing the PML in the domain Ω_∞. In terms of shape functions v_k $(k=1,2,\cdots)$, it follows that

$$\begin{aligned}&\iint_\Omega v_1\left\{\nabla\cdot(cc_g\nabla\zeta)+(m\omega)^2\left(\frac{c_g}{c}-i\tilde{f}_d\right)\zeta-Q\right\}d\Omega\\&+\iint_{\Omega_\infty}v_2\left\{\begin{array}{l}\nabla_1\left(\frac{\lambda_2}{\lambda_1}cc_g\nabla_1\zeta^\infty\right)+\nabla_2\left(\frac{\lambda_1}{\lambda_2}cc_g\nabla_2\zeta^\infty\right)\\+(m\omega)^2\left(\frac{c_g}{c}-i\tilde{f}_d\right)\lambda_1\lambda_2\zeta^\infty\end{array}\right\}d\Omega_\infty\\&+\int_\Gamma v_{31}(\zeta-\zeta^\infty)ds+\int_\Gamma v_{32}(\boldsymbol{n}\cdot\nabla\zeta+\boldsymbol{n}_\infty\cdot\nabla\zeta^\infty)ds\\&+\int_{\Gamma_B}v_4(\boldsymbol{n}_B\cdot\nabla\zeta-B\zeta)ds\\&+\int_{\Gamma_D}v_5\left\{[cc_g\boldsymbol{n}_D\cdot\nabla\zeta]_{\xi_0^-}^{\xi_0^+}-D\zeta\right\}ds=0.\end{aligned} \tag{A.19}$$

The first and second domain integrals in Eq. (A.19) are transformed, with the aid of Green's formula, into the weak forms as follows:

(1) The first integral in Ω:

$$I=-\iint_\Omega\left\{\begin{array}{l}cc_g\nabla v_1\cdot\nabla\zeta-v_1(m\omega)^2\left(\frac{c_g}{c}-i\tilde{f}_d\right)\zeta\\+v_1Q\end{array}\right\}d\Omega+\int_{\Gamma+\Gamma_B+\Gamma_D\,in\,\Omega}v_1cc_g\boldsymbol{n}\cdot\nabla\zeta ds. \tag{A.20}$$

(2) The second integral in Ω_∞:

$$I_\infty=-\iint_{\Omega_\infty}\left\{\begin{array}{l}\frac{\lambda_2}{\lambda_1}cc_g\nabla_1v_2\,\nabla_1\zeta^\infty+\frac{\lambda_1}{\lambda_2}cc_g\nabla_2v_2\,\nabla_2\zeta^\infty\\-v_2(m\omega)^2\left(\frac{c_g}{c}-i\tilde{f}_d\right)\lambda_1\lambda_2\zeta^\infty\end{array}\right\}d\Omega_\infty$$

$$+\int_{\Gamma+\Gamma_\infty}\left\{n_1\left(v_2cc_g\frac{\lambda_2}{\lambda_1}\nabla_1\zeta^\infty\right)+n_2\left(v_2cc_g\frac{\lambda_1}{\lambda_2}\nabla_2\zeta^\infty\right)\right\}ds, \tag{A.21}$$

where (n_1,n_2) are the components of the vector $\boldsymbol{n}_\infty$. Inserting Eqs. (A.20) and (A.21) into Eq. (A.19) leads

$$\begin{aligned}&\iint_\Omega\left\{cc_g\nabla v_1\cdot\nabla\zeta-v_1(m\omega)^2\left(\frac{c_g}{c}-i\tilde{f}_d\right)\zeta+v_1Q\right\}d\Omega\\&+\iint_{\Omega_\infty}\left\{\begin{array}{l}\frac{\lambda_2}{\lambda_1}cc_g\nabla_1v_2\,\nabla_1\zeta^\infty+\frac{\lambda_1}{\lambda_2}cc_g\nabla_2v_2\,\nabla_2\zeta^\infty\\-v_2(m\omega)^2\left(\frac{c_g}{c}-i\tilde{f}_d\right)\lambda_1\lambda_2\zeta^\infty\end{array}\right\}d\Omega_\infty\\&-\int_\Gamma\left\{\begin{array}{l}v_1cc_g\boldsymbol{n}\cdot\nabla\zeta\\+\left\{n_1\left(v_2cc_g\frac{\lambda_2}{\lambda_1}\nabla_1\zeta^\infty\right)+n_2\left(v_2cc_g\frac{\lambda_1}{\lambda_2}\nabla_2\zeta^\infty\right)\right\}\\+v_{31}(\zeta-\zeta^\infty)+v_{32}(\boldsymbol{n}\cdot\nabla\zeta+\boldsymbol{n}_\infty\cdot\nabla\zeta^\infty)\end{array}\right\}ds\\&-\int_{\Gamma_\infty}\left\{n_1\left(v_2cc_g\frac{\lambda_2}{\lambda_1}\nabla_1\zeta^\infty\right)+n_2\left(v_2cc_g\frac{\lambda_1}{\lambda_2}\nabla_2\zeta^\infty\right)\right\}ds\\&-\int_{\Gamma_B}\{v_1cc_g\boldsymbol{n}\cdot\nabla\zeta+v_4(\boldsymbol{n}_B\cdot\nabla\zeta-B\zeta)\}ds\\&-\int_{\Gamma_D}\left\{v_1cc_g\boldsymbol{n}\cdot\nabla\zeta+v_5\left([cc_g\boldsymbol{n}_D\cdot\nabla\zeta]_{\xi_0^-}^{\xi_0^+}-D\zeta\right)\right\}ds=0.\end{aligned} \tag{A.22}$$

In addition, with respect to the curvilinear integral along Γ_D in Eq. (A.22), as shown by the broken line in Fig. A.1, the cut made on the line Γ_D divides this path of integration into Γ_D^+ and Γ_D^-, and then the curvilinear integral along the line Γ_D becomes

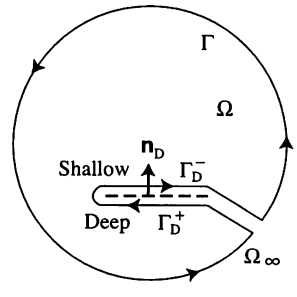

Fig. A.1 Curvilinear integral along the line of water depth discontinuity.

$$\begin{aligned}&\int_{\Gamma_D}v\varphi\boldsymbol{n}\cdot\nabla\psi ds\\&=\int_{\Gamma_D^+}v\varphi\boldsymbol{n}_D\cdot\nabla\psi ds+\int_{\Gamma_D^-}v\varphi(-\boldsymbol{n}_D)\cdot\nabla\psi ds\\&=\int_{\Gamma_D}v[\varphi\boldsymbol{n}_D\cdot\nabla\psi]_{\xi_0^-}^{\xi_0^+}ds.\end{aligned} \tag{A.23}$$

Thus, the last term in Eq. (A.22) is replaced by

$$I_D=\int_{\Gamma_D}\left\{v_1[cc_g\boldsymbol{n}\cdot\nabla\zeta]_{\xi_0^-}^{\xi_0^+}+v_5\left([cc_g\boldsymbol{n}_D\cdot\nabla\zeta]_{\xi_0^-}^{\xi_0^+}-D\zeta\right)\right\}ds. \tag{A.24}$$

To satisfy the boundary conditions, the derivatives of free surface displacement, $\nabla\zeta$ and $\nabla\zeta^\infty$, in the curvilinear integrals in Eqs. (A.22) and (A.24) are eliminated.

(a) On the line Γ:

The condition $\zeta=\zeta^\infty$ is the natural boundary condition

on the line Γ, which is satisfied by the PML. Taking account of $\lambda_1 = 1$ and $\lambda_2 = 1$ on the line Γ and thus $n_1\nabla_1\zeta^{\infty} + n_2\nabla_2\zeta^{\infty} = \boldsymbol{n}_{\infty}\cdot\nabla\zeta^{\infty}$, set $v_{32} = -v_2 cc_g$ to eliminate $\boldsymbol{n}_{\infty}\cdot\nabla\zeta^{\infty}$, and further setting $v_2 = v_1$ yields

$$\int_{\Gamma}(\cdots)ds = \int_{\Gamma}\{(v_1 - v_2)cc_g\boldsymbol{n}\cdot\nabla\zeta\}ds = 0. \quad \text{(A.25)}$$

(b) On the line Γ_{∞}:

In order for the PML to be effective, waves are required to decay exponentially on the way to the line Γ_{∞} in the far-field. This leads $\zeta^{\infty} \to 0$, $\nabla_1\zeta^{\infty} \to 0$, and $\nabla_2\zeta^{\infty} \to 0$; thus, the curvilinear integral along Γ_{∞} vanishes. The PML is therefore exploitable as a replacement of the far-field radiation condition (SRC, Eq. (A.18)).

(c) On the line Γ_B:

Taking account of $\boldsymbol{n}_B = \boldsymbol{n}$ in Ω, set $v_{41} = -v_1 cc_g$ to eliminate $\boldsymbol{n}_B\cdot\nabla\zeta$, and then

$$\int_{\Gamma_B}(\cdots)ds = \int_{\Gamma_B} v_1 cc_g B\zeta\, ds. \quad \text{(A.26)}$$

(d) On the line Γ_D:

In Eq. (A.24) instead of the last term in Eq.(A.22), taking account of $\boldsymbol{n}_D = \boldsymbol{n}$ in Ω, set $v_{51} = -v_1$ to eliminate $\boldsymbol{n}_D\cdot\nabla\zeta$, and then

$$\int_{\Gamma_D}(\cdots)ds = \int_{\Gamma_D} v_1 D\zeta\, ds. \quad \text{(A.27)}$$

With the the discussions (a)-(d) above, the weak form (A.22) for FEM becomes

$$\begin{aligned}
&\iint_{\Omega}\left\{cc_g\nabla v_1\cdot\nabla\zeta - v_1(m\omega)^2\left(\frac{c_g}{c} - i\tilde{f}_d\right)\zeta + v_1 Q\right\}d\Omega \\
&+\iint_{\Omega_{\infty}}\begin{bmatrix}\dfrac{\lambda_2}{\lambda_1}cc_g\nabla_1 v_1\,\nabla_1\zeta^{\infty} + \dfrac{\lambda_1}{\lambda_2}cc_g\nabla_2 v_1\,\nabla_2\zeta^{\infty} \\ -v_1(m\omega)^2\left(\dfrac{c_g}{c} - i\tilde{f}_d\right)\lambda_1\lambda_2\zeta^{\infty}\end{bmatrix}d\Omega_{\infty} \\
&-\int_{\Gamma_B} v_1 cc_g B\zeta ds - \int_{\Gamma_D} v_1 D\zeta\, ds = 0. \quad \text{(A.28)}
\end{aligned}$$

2.2 One-dimensional problems

If the PMLs are set up on the both sides, in Ω_{∞} and $\Omega_{-\infty}$, of the domain of analysis Ω, as shown in Fig. 4.2, and it is assumed that waves are incident from the offshore domain Ω_{∞}. Similar to Eq. (A.22), the weak form for FEM is given as follows:

$$\begin{aligned}
&\int_{\Omega}\left\{cc_g\nabla v_1\nabla\zeta - v_1(m\omega)^2\left(\frac{c_g}{c} - i\tilde{f}_d\right)\zeta + v_1 Q\right\}d\Omega \\
&+\int_{\Omega_{\infty}}\left\{\frac{cc_g}{\lambda}\nabla v_2\,\nabla\zeta^{\infty} - v_2(m\omega)^2\left(\frac{c_g}{c} - i\tilde{f}_d\right)\lambda\zeta^{\infty}\right\}d\Omega_{\infty} \\
&-\left|\begin{matrix}v_1 cc_g\boldsymbol{n}\cdot\nabla\zeta + n\left(v_2\dfrac{cc_g}{\lambda}\nabla\zeta^{\infty}\right) \\ +v_{31}(\zeta - \zeta^{\infty}) + v_{32}(\boldsymbol{n}\cdot\nabla\zeta + \boldsymbol{n}_{\infty}\cdot\nabla\zeta^{\infty})\end{matrix}\right|_{\Gamma} \\
&-\left|n\left(v_2\frac{cc_g}{\lambda}\nabla\zeta^{\infty}\right)\right|_{\Gamma_{\infty}} \\
&+\int_{\Omega_{-\infty}}\left\{\frac{cc_g}{\lambda}\nabla v_2\,\nabla\zeta^{-\infty} - v_2(m\omega)^2\left(\frac{c_g}{c} - i\tilde{f}_d\right)\lambda\zeta^{-\infty}\right\}d\Omega_{-\infty}
\end{aligned}$$

$$\begin{aligned}
&-\left|\begin{matrix}v_1 cc_g\boldsymbol{n}\cdot\nabla\zeta + n\left(v_2\dfrac{cc_g}{\lambda}\nabla\zeta^{-\infty}\right) \\ +v_{31}(\zeta - \zeta^{-\infty}) + v_{32}(\boldsymbol{n}\cdot\nabla\zeta + \boldsymbol{n}_{\infty}\cdot\nabla\zeta^{-\infty})\end{matrix}\right|_{\Gamma_-} \\
&-\left|n\left(v_2\frac{cc_g}{\lambda}\nabla\zeta^{-\infty}\right)\right|_{\Gamma_{-\infty}} \\
&-\left|v_1 cc_g\boldsymbol{n}\cdot\nabla\zeta + v_4(\boldsymbol{n}_B\cdot\nabla\zeta - B\zeta)\right|_{\Gamma_B} \\
&-\left|v_1 cc_g\boldsymbol{n}\cdot\nabla\zeta + v_5\left([cc_g\boldsymbol{n}_D\cdot\nabla\zeta]_{\xi_0^-}^{\xi_0^+} - D\zeta\right)\right|_{\Gamma_D}.
\end{aligned} \quad \text{(A.29)}$$

Through the discussion similar to (a)-(d) for the two-dimensional problems, the boundary terms on Γ, Γ_{∞}, Γ_-, and $\Gamma_{-\infty}$ vanish, and then we have

$$\begin{aligned}
&\int_{\Omega}\left\{cc_g\nabla v_1\nabla\zeta - v_1(m\omega)^2\left(\frac{c_g}{c} - i\tilde{f}_d\right)\zeta + v_1 Q\right\}d\Omega \\
&+\int_{\Omega_{\infty}}\left\{\frac{cc_g}{\lambda}\nabla v_1\,\nabla\zeta^{\infty} - v_1(m\omega)^2\left(\frac{c_g}{c} - i\tilde{f}_d\right)\lambda\zeta^{\infty}\right\}d\Omega_{\infty} \\
&+\int_{\Omega_{-\infty}}\left\{\frac{cc_g}{\lambda}\nabla v_1\,\nabla\zeta^{-\infty} - v_1(m\omega)^2\left(\frac{c_g}{c} - i\tilde{f}_d\right)\lambda\zeta^{-\infty}\right\}d\Omega_{-\infty} \\
&-\left|v_1 cc_g B\zeta\right|_{\Gamma_B} - \left|v_1 cc_g D\zeta\right|_{\Gamma_D} = 0. \quad \text{(A.30)}
\end{aligned}$$

On the other hand, if the wave field in the offshore domain Ω_{∞} is assumed to be linear, the radiative boundary condition can be used at the end-side of the domain of analysis. Thus the PML is set up only on the transmission side, in $\Omega_{-\infty}$, of the domain of analysis. Similar to Eq. (A.22), the weak form for FEM is given as follows:

$$\begin{aligned}
&\int_{\Omega}\left\{cc_g\nabla v_1\nabla\zeta - v_1(m\omega)^2\left(\frac{c_g}{c} - i\tilde{f}_d\right)\zeta + v_1 Q\right\}d\Omega \\
&-\left|v_1 cc_g\boldsymbol{n}\cdot\nabla\zeta\right|_{\Gamma} \\
&+\int_{\Omega_{-\infty}}\left\{\frac{cc_g}{\lambda}\nabla v_2\,\nabla\zeta^{-\infty} - v_2(m\omega)^2\left(\frac{c_g}{c} - i\tilde{f}_d\right)\lambda\zeta^{-\infty}\right\}d\Omega_{-\infty} \\
&-\left|\begin{matrix}v_1 cc_g\boldsymbol{n}\cdot\nabla\zeta + n\left(v_2\dfrac{cc_g}{\lambda}\nabla\zeta^{-\infty}\right) \\ +v_{31}(\zeta - \zeta^{-\infty}) + v_{32}(\boldsymbol{n}\cdot\nabla\zeta + \boldsymbol{n}_{\infty}\cdot\nabla\zeta^{-\infty})\end{matrix}\right|_{\Gamma_-} \\
&-\left|n\left(v_2\frac{cc_g}{\lambda}\nabla\zeta^{-\infty}\right)\right|_{\Gamma_{-\infty}} \\
&-\left|v_1 cc_g\boldsymbol{n}\cdot\nabla\zeta + v_4(\boldsymbol{n}_B\cdot\nabla\zeta - B\zeta)\right|_{\Gamma_B} \\
&-\left|v_1 cc_g\boldsymbol{n}\cdot\nabla\zeta + v_5\left([cc_g\boldsymbol{n}_D\cdot\nabla\zeta]_{\xi_0^-}^{\xi_0^+} - D\zeta\right)\right|_{\Gamma_D} = 0.
\end{aligned} \quad \text{(A..31)}$$

In this case, the boundary terms on Γ_- and $\Gamma_{-\infty}$ vanish, and then we have

$$\begin{aligned}
&\int_{\Omega}\left\{cc_g\nabla v_1\nabla\zeta - v_1(m\omega)^2\left(\frac{c_g}{c} - i\tilde{f}_d\right)\zeta + v_1 Q\right\}d\Omega \\
&+\int_{\Omega_{-\infty}}\left\{\frac{cc_g}{\lambda}\nabla v_2\,\nabla\zeta^{-\infty} - v_2(m\omega)^2\left(\frac{c_g}{c} - i\tilde{f}_d\right)\lambda\zeta^{-\infty}\right\}d\Omega_{-\infty} \\
&-\left|v_1 cc_g B\zeta\right|_{\Gamma_B} - \left|v_1 cc_g D\zeta\right|_{\Gamma_D} = \left|v_1 cc_g\boldsymbol{n}\cdot\nabla\zeta\right|_{\Gamma}. \quad \text{(A.32)}
\end{aligned}$$